# Historical resurgences after tropical cyclones in the Mid-Atlantic Bight: A primary mechanism and hotspot

Tam T. Trinh[a], Philip M. Orton[a], Mahmoud Ayyad[a], Charitha Pattiaratchi[b], Stefan A. Talke[c]

[a] Department of Civil, Environmental and Ocean Engineering, Stevens Institute of Technology, Hoboken, NJ, United States

[b] UWA Oceans Institute, University of Western Australia, Perth, Australia

[c] Department of Civil and Environmental Engineering, California Polytechnic State University, San Luis Obispo, CA, United States

*Keywords: resurgence, storm surge, coastal flooding, continental shelf seiche, edge wave, tropical cyclone, New York Bight*

## Highlights

- Historical data analysis indicates the New York Bight is a hotspot for “resurgence”
- Resurgence trough-to-crest heights were up to 1.5 m, with a wave period of 7-8 h
- Idealized modeling demonstrates the predominant mechanism at NYB is a shelf seiche
- Down-coast movement occurs as Kelvin waves, disappears without the Coriolis effect

## Abstract

After a storm surge, non-tidal oscillations known as resurgences often occur independently of continued meteorological forcing and have at times been attributed to either edge waves or continental shelf seiches. Our wavelet-based evaluation of New York Harbor tide-gauge records (1860-2024) shows that resurgences with 7-8 h periods and amplitudes of up to 1.5 m have been observed following hurricanes in the New York Bight (NYB) in 29 of 112 observed tropical cyclones (26%). A comparison of 17 coastal tidal gauges across the Mid-Atlantic Bight shows that the oscillations in the NYB are anomalously large compared to other regions. Linear regression reveals that resurgence amplitude is positively correlated with storm surge, maximum sustained wind speed and northward storm propagation speed. These results motivate further exploration of resurgence mechanisms using numerical simulations with idealized onshore wind forcing that abruptly stops, similar to the winds after a fast-moving hurricane passes. Simulations both with and without Coriolis produce nearly synchronous water level fluctuations across the NYB shelf, indicative of a localized standing wave. Cross-correlation analysis of the model results reveals waves propagating unidirectionally down the coast, but at speeds inconsistent with those of edge waves, and only when the Coriolis effect is present. Our study concludes that the resurgence in the NYB is primarily a standing wave oscillating at the shelf resonant frequency. Thus, the predominant mechanism of this resurgence is a continental shelf seiche, with energy trapped and amplified in the NYB by the concave coastal geometry, with energy loss down-coast by Kelvin waves.


## 1. Introduction

Coastal flooding can cause significant damage, particularly in regions with dense populations and valuable infrastructure. Flooding results from a variety of different causes, including tides (Eliot, 2010; Marsooli & Wang, 2020; Orton et al., 2012), wind and wave setup (Dodet et al., 2019; Leijala et al., 2018; Staneva et al., 2016), and atmospheric pressure gradients (Pugh & Woodworth, 2014), which can be exacerbated by rainfall and river inputs (Orton et al., 2012). A well-known, storm-driven cause of coastal flooding is storm surge, caused, for example, by strong onshore or alongshore winds from a tropical cyclone (TC) combined with low atmospheric pressure, pushing seawater toward the shore (Pugh & Woodworth, 2014). Although storm surges are a primary driver of flooding along the Atlantic Coast, they are not the only contributing factors to flooding. For example, the forerunner increases the water level as the storm approaches the coast (Trinh et al., 2020). Redfield and Miller (1957) identified 'resurgence' as an additional storm-related mechanism influencing coastal water levels. Resurgence is defined as oscillations of the coastal water levels subsequent to the passage of a storm (Redfield & Miller, 1957). The authors stressed the importance of resurgence, as it is a sudden increase in water levels that can occur just when a storm appears to be ending. More significantly, Redfield and Miller (1957) cautioned that resurgence could present future risks to coastal communities. For example, a resurgence in 2020 unexpectedly triggered minor coastal flooding in New York Harbor (NYH) and surrounding local areas during and after the passage of Hurricane Isaias 2020 (Ayyad et al., 2022). The resurgence occurred after the storm's center had passed, and winds had subsided, as had been warned decades before.

Multiple mechanisms have been proposed to explain the physical causes of resurgence. In one interpretation, the resurgence is explained by edge waves generated by a travelling disturbance over the continental shelf (Munk et al., 1956). The phase velocity, wavelength, and period of the resurgence over a continental shelf with constant slope were calculated using a linear wave theory adapted from the classical theory describing wave propagation over uniformly sloping bathymetry, specifically, the edge wave formulation developed by Ursell (1952). Not long after, Greenspan (1956) used an analytical model to calculate the wavelengths, frequencies, and amplitudes of the resurgent wave motion induced by pressure disturbance moving parallel to a straight coastline and concluded that resurgence is the fundamental mode of edge waves (see also Wijeratne & Pattiaratchi, 2024).

In another interpretation, the mechanism of water level resurgence is a shelf (or "coastal") seiche oscillating in a direction normal to the coastline. A shelf seiche can form when a storm-induced free wave reflects back and forth across the continental shelf (Redfield & Miller, 1957). Shelf seiches involve reflection off the coast and a phase-shifted reflection off the shelf break (Vennell, 2010). When a storm passes and the wind subsides, the storm surge retreats toward the open ocean, back across the shelf. Hope et al. (2013) reported that resonant, reflected long waves were observed across the wide continental shelf in Louisiana and Texas Gulf Coast, with a 12-h seiche period matching the shelf's natural resonance and interacting with and amplifying the semidiurnal tides. The sharp bathymetric transition at the continental shelf break triggers an out-of-phase reflection of the surge back onto the shelf (Hope et al., 2013). When a wave crosses a step change in depth, reflected and refracted waves are generated, and the amplitudes of the two depend on the relative depth (Pasquet & Vilibić, 2013). The difference in depth determines the amount of energy retained by these reflected waves, and larger depth contrasts result in stronger reflections. A survey of Pasquet et al. (2013) of sites along the US East Coast reported the presence of topographically trapped edge waves and standing waves with periods up to 6 hours, which can contribute to significant wave heights of up to 100 cm. Continental shelf seiches have also been observed on the Argentine shelf (Mysak, 1980) along the Australian shelf (Pattiaratchi et al., 2022), and on the Caribbean Coast (Huang et al., 2000).

In this study, we investigate resurgences in the New York Bight using an unusually long time series of hourly datasets from 1860 to the present (Talke et al., 2014), enabling the reanalysis of the Munk et al. (1956) resurgences with improved tools and observations at 17 locations from Nantucket Island in the North to Duck in the South. We utilize wavelet transforms to detect significant resurgences and quantify their characteristics, evaluate the spatial-temporal development of resurgences, and determine their relation to storm parameters via linear regression and cross-correlation. Also, we employ numerical modeling with idealized onshore shelf-wide wind forcing to assess the intrinsic shelf frequency and dynamical behavior of resurgence waves. Our objective is to establish a set of criteria to quantify resurgences in the time series of water levels, study the mechanism behind the phenomenon, and evaluate the primary factors influencing its amplitude, period, and duration.

The paper is structured as follows: Section 2 details the methodology. Section 3 presents the results. Section 4 discusses the resurgence mechanisms and controls on resurgence characteristics. The paper closes in Section 5 with a summary and conclusions.

## 2. Methodology

### 2.1. Study area

The New York Bight (NYB) is situated along the Atlantic coast of the United States as a part of the Mid-Atlantic Bight that extends from Cape May in the south to Montauk in the north (Figure 1). The continental shelf, defined here as depths < 200 m, reaches its maximum cross-shelf width of ~200 km from Sandy Hook to the shelf break, gradually narrowing down to ~105 km in the southern New Jersey shelf near Ocean City Inlet station. The study area includes a total of 17 tide gauges to study the spatial development of resurgence (Figure 1).

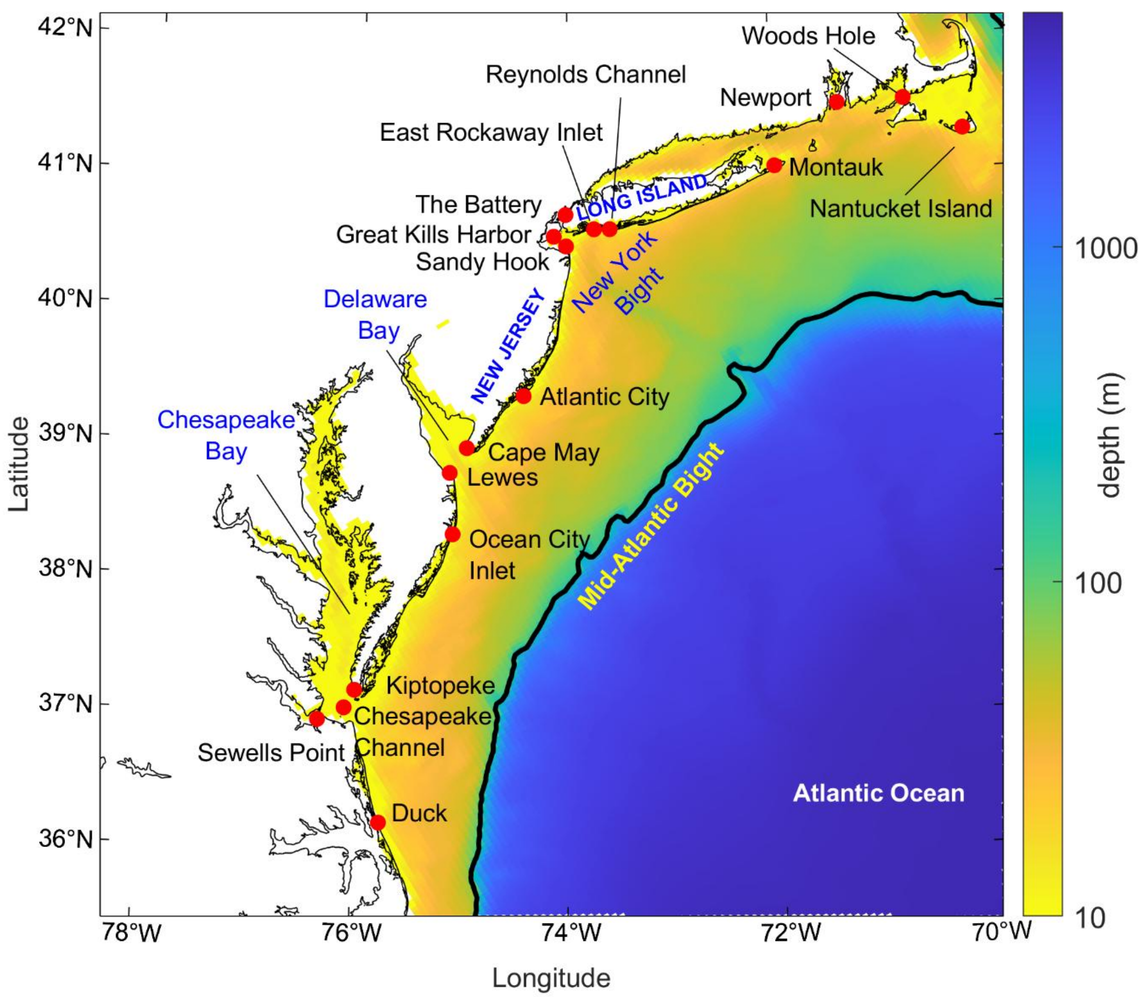


**Fig. 1.** Study area and its bathymetry showing 17 tide gauges (red dots) along the NYB and the Mid-Atlantic Bight. The thick black line represents the 200-m depth contour.

## 2.2. Data

### *2.2.1. Water-level observations*

We used two sets of time series of water level observations: (1) single-gauge time series; and (2) a composite "New York Harbor" time series from 1860 to 2024. Hourly water level observations along the U.S. East Coast are obtained from the National Oceanographic and

Atmospheric Administration (NOAA) and the United States Geological Survey (USGS) from URLs noted in the Data Availability section. Here, we evaluate 17 long-term tide gauges within the NYB and the Mid-Atlantic Bight region, which are available from NOAA and USGS (see Figure 1 and Supplemental Table S1). Stations such as The Battery, Sandy Hook, and Sewells Point have been recording water levels for over a century, with records dating back to the late 1800s and early 1900s. Meanwhile, other stations, such as Reynolds Channel, East Rockaway Inlet, Great Kills Harbor, Ocean City Inlet, and Chesapeake Channel, began monitoring only a few decades ago.

For NYH water levels, we use a near-continuous, hourly composite "New York Harbor" dataset from 1860 to 2024 compiled from data collected at Governors Island, the Hamilton Ferry Dock in Brooklyn, Fort Hamilton, NY, The Battery, NY, and Sandy Hook, NJ, of which all but the latter are within 10 km of The Battery (within or at the edge of Upper NY Bay; (see details in Talke et al., 2014). The purpose of applying the composite datasets is to create a relatively uniform and complete dataset for as much of the available historical hurricane track record (1851-present) as possible. Talke et al. (2014) evaluated instrument evolution, uncertainties, and data homogenization for the long-term record used in this study. Except for a period from roughly September 1882-1885, hourly records contained few gaps and were considered of excellent quality, consistent with other studies of historical tidal records (e.g., Talke et al., 2020). Beginning in the mid-19$^{th}$ century, historical hourly records were transcribed from continuous measurements on rolls of paper known as marigrams, and checked daily by on-site tidal observers (e.g., Latapy et al., 2023; Talke & Jay, 2013; Talke & Jay, 2017). Therefore, quantitative analysis of 19th and early 20$^{th}$ century data shows that data quality is comparable to and often exceeds mid-20th century records (see e.g., Ray & Talke, 2019; Talke et al., 2018; Talke et al., 2020). Thus, our use of historical records is reasonable and enables a more complete statistical study of an important, but relatively infrequent, phenomenon. We also note that our wavelet-based methodology (see below) is a good tool for evaluating non-stationary tidal and non-tidal processes, assessing intermittent gauge noise (including sudden offsets), and filtering the signal (see e.g., Jay & Flinchem, 1997; Lobo et al., 2024); here, we detected no evidence that data issues were influencing our analysis.

#### *2.2.2. Hurricane data*

We utilize the Atlantic hurricane database (HURDAT2) (Landsea & Franklin, 2013) from the National Hurricane Center and Central Pacific Hurricane Center - NOAA, spanning from 1851 to 2024 (https://www.nhc.noaa.gov/data/), which contains the "best track" information for historical hurricanes. This dataset provides six-hourly observations of location, maximum winds, and central pressure, enabling the quantification of hurricane characteristics. For the period from 1860 to 2024, 116 TCs passed within a 250 km radius of Sandy Hook. However, due to overlapping with hourly water level observations at NYH, 112 TCs are used to quantify TC characteristics and analyze the relationship between storm parameters and resurgence characteristics.

### 2.3. Data analysis

A non-tidal residual (NTR) is computed by removing annual mean sea level and tidal predictions from the total water level observations with year-by-year tidal harmonic analysis, using T-TIDE developed by Pawlowicz et al. (2002). For partial years of data, tidal harmonic constituents are extracted through a month-by-month analysis.

#### *2.3.1. Wavelet transform analysis and criteria used to identify resurgences*

Focusing on periods when hurricanes were within 250 km of NYH, the continuous wavelet transform (CWT) is used to detect resurgences and calculate their period, amplitude, and decay timescale. CWT is an analysis tool like the Fourier Transform, which returns the signal components in the frequency domain. However, unlike the Fourier Transform, CWT returns a two-dimensional result, yielding a time-frequency representation of signals that provides information in both the frequency and time domains (Torrence & Compo, 1998). Therefore, CWT is useful for periodic processes that have time-variation in energy at each frequency and has been applied recently in studies of tide gauge data for meteotsunamis (Dusek et al., 2019; Kim et al., 2022; Kim & Omira, 2024; Linares et al., 2016). In this study, resurgences are periodic events that are localized in time; thus, the wavelet transform is an ideal tool for their quantification. We apply the analytic Morse wavelet, with the symmetry parameter, gamma ($\gamma$), equal to 3.0, and the time-bandwidth product equal to 60 (Lilly & Olhede, 2012). These settings result in a wavelet with no skewness, five wave cycles, and good frequency localization.

Searching the period when a TC is within 250 km of NYH, we detect the time of maximum NTR, which sets our time frame for analysis of each storm. The window for wavelet analysis was defined as 1.0 day before the NTR peak to 4.0 days afterwards. The resulting scalograms display the shading of the magnitude (absolute value) of the wavelet transform, which is versus the period and time in the y- and x-axes, respectively.

For each of the 112 hurricane storm surge events evaluated, we use the following two criteria to identify the common pattern we refer to as a 'resurgence':

(1) **Local maxima** in wavelet magnitude above the noise floor are detected in the scalogram following the NTR peak. The noise floor is conservatively defined as five standard deviations above the mean of the scalogram in the selected bands, based on the last ten years of data.

(2) **The period** of the local maxima in wavelet magnitude ranges between 4 and 9 h.

The selection of resurgence band periods, ranging from 4 to 9 h, is locally appropriate for the NYB and informed by prior studies (e.g., Ayyad et al., 2022; Greenspan, 1956; Munk et al., 1956; Redfield & Miller, 1957). It is designed to minimize interference from meteotsunamis (with periods ranging from 2 min to 2 h, as reported by Dusek et al. (2019) and from residual semidiurnal tidal energy in the NTR time series (12.42 h). These two criteria successfully identify previously studied resurgence events in 1938, 1944, 1954, 1960, 1985, and 2020, as reported in the research of Ayyad et al. (2022) and Munk et al. (1956).

The decay timescale of the resurgence amplitude envelope is estimated based on the e-folding time for the time series of wavelet response magnitude at the period of the local maximum (see Section 3.2 for an example result using the 1944 hurricane). E-folding time is defined as the time interval in which an exponentially growing quantity increases by a factor of Euler's number (e); here, it is the required time for the amplitude to decline to 1/e (~36.8%) of its maximum value. The e-folding is used as a standard metric for characterizing temporal or spatial decay. This measure has been employed to quantify the temporal timescale of forced and free waves (e.g., Qiu et al., 1997), tsunamis (e.g., Devlin et al., 2023; Rabinovich et al., 2013).

#### ***2.3.2. Regression of resurgence characteristics with storm surge and storm-forcing variables***

To investigate the storm-related causes and controls of resurgences, we linearly regress their empirically determined characteristics (amplitude, period, and decay timescale) against the maximum storm surge and storm forcing variables obtained from HURDAT2, including storm intensity, storm path, maximum sustained wind speed, and storm propagation speed. A robust fitting method, which is less sensitive to outliers in the data compared to ordinary least squares regression, is used to reduce the influence of outliers (e.g., storm surge during Hurricane Sandy in 2012) (Pérez et al., 2014). All HURDAT records are interpolated to hourly timesteps, and storm propagation speed is split into northerly and easterly components. The approach angle is defined as the direction of the hurricane track in its last timestep before passing the latitude of Sandy Hook, measured clockwise from the North. For the distance east of Sandy Hook, distances are measured positively (negatively) in the eastward (westward) direction.

### **2.4. Numerical modeling and model data analysis**

Numerical modeling with idealized wind forcing and no tidal forcing on a realistic ocean domain is applied here to enhance our understanding of the detailed spatiotemporal evolution of the NYB resurgence, as well as its mechanisms.

#### ***2.4.1. Hydrodynamic model and domain***

We utilize the three-dimensional Stevens Institute Estuarine and Coastal Ocean Hydrodynamic Model (sECOM) with idealized wind forcing (Blumberg & Georgas, 2008; Georgas, Yin, et al., 2016). The model is a free-surface, hydrostatic, hydrodynamic model with terrain-following (sigma) vertical coordinates set on an orthogonal, curvilinear Arakawa C-grid. The model is applied on the SNAP (Stevens Northwest Atlantic Predictions) domain with a rectangular 4 x 6 km resolution, 300 x 300 grid extending from the Gulf of St. Lawrence to Cape Hatteras and approximately 2000 km offshore (Jordi et al., 2019; Orton et al., 2016). It runs in three-dimensional mode, with ten vertical sigma layers and a bottom drag coefficient of 0.0025. SNAP has constant temperature and stratification; thus, the simulation ignores baroclinic forcing. In addition, SNAP has a radiating water level boundary condition, and here, the water level is set to zero instead of its normal approach of an inverse barometer-based water level (Reid & Bodine, 1968). Past quality assurance for sECOM on the SNAP domain has demonstrated typical operational forecast water level errors of ~0.10-0.15 m (Georgas, Yin, et al., 2016). It has been a component of the Stevens Flood Advisory System since late 2015 (Ayyad et al., 2022; Georgas, Blumberg, et al., 2016)

#### ***2.4.2. Idealized resurgence simulations***

The sECOM-SNAP model is applied with forcing only from a southeast wind blowing only over the NYB continental shelf (Figure 1), ramping up to ~ 28 m $s^{-1}$ over 6 h, then holding constant for 18 h, then rapidly dropping to zero over 30 min. The window of the onshore wind forcing stretches from Lewes to Montauk and offshore beyond the edge of the continental shelf (Figures 1 & 7). Winds are spatially smoothed at the edges to avoid an abrupt change to zero. The simulation period for the idealized wind-forcing case of resurgence is set to 5.0 days, effectively capturing the decay timescale of the resurgence. This duration helps assess whether the decay follows the same trend observed in water level observations. An additional experiment, excluding the Coriolis force, is simulated to isolate its effects on the resurgence dynamics. An overview of the experimental cases is provided in Table 1. We refer to the experiment without the Coriolis effect as the 'non-Coriolis experiment' throughout this paper.

**Table 1.** Summary of numerical experimental simulations

| ***Experiments*** | ***Coriolis force*** | ***Expected dynamic behavior*** | ***Objective*** |
|---|---|---|---|
| ***Control*** | *Yes* | *Alongshore movement, geostrophic balance, and sea level gradients are influenced by the Earth's rotation.* | *To simulate realistic coastal dynamics influenced by the Earth's rotation.* |
| ***Non-Coriolis*** | *No* | *Suppresses alongshore motion; highlights non-rotational contributions; and alters sea level patterns.* | *To isolate Coriolis effects and quantify the role of the Coriolis force in water level variations.* |

#### *2.4.3. Quantitative analysis of the correlation and time lag*

Edge waves and shelf seiches exhibit distinct physical behaviors: Edge waves travel along the coastline and can travel in both directions away from the landfall location of TCs (Pattiaratchi et al., 2022; Yankovsky, 2009), whereas continental shelf seiches are standing wave oscillations involving reflection of a wave back and forth across the shelf (Pugh & Woodworth, 2014, p. 167). To assess whether traveling waves exist within the study area, we employ cross-correlation analysis on the modeled water level data at several locations along the open coast, relative to Sandy Hook, from model time day 1.25 to 5.0. Given the oscillating resurgence behavior, any areas with a strong maximum cross-correlation (at any lag) are subjected to the same wave behavior. Suppose a strong correlation is observed at a certain time lag. In that case, it may indicate the presence of edge waves or other types of traveling waves, as well as their direction of propagation toward the reference point (Sandy Hook). If the NYB region displays consistently high correlations with a near-zero time lag, this pattern can indicate a standing wave or a shelf seiche.

## 3. Results

### 3.1. Spatial pattern of historical East Coast resurgence events

The spatial pattern of the NTR for several storms is presented over 5.0 days to capture the peak and evolution of resurgences at selected stations. Here, we present the spatial and temporal evolution of the NTR for eight historical resurgence events, which are displayed across 3-17 tidal records (Figure 2). Resurgences in some historical hurricanes, including the 1938 Great New England Hurricane, the 1944 Great Atlantic Hurricane, and Hurricane Carol in 1954 (reported in Munk et al. (1956), had heights (trough to crest) similar to the wave heights of the primary surge produced by onshore winds. In the 1938 Great New England Hurricane, the resurgence height reached ~1.5 m at Sandy Hook and 1.2 m at The Battery, resulting in non-tidal residuals of 0.45 m and 0.65 m, respectively. Meanwhile, the storm surge was ~1.0 m at Sandy Hook and ~1.2 m at The Battery (Figure 2a). In the 1944 Great Atlantic Hurricane, both the storm surge and the resurgence's peak NTR values were ~1.0 m. In contrast, for Hurricane Carol in 1954, the resurgence peak NTR, at 0.95 m, was higher than the primary storm surge, at 0.75 m, at The Battery (Figure 2b and c, respectively). Both of these hurricanes produced multiple peaks at The Battery and Sandy Hook, with each subsequent peak declining in amplitude until they eventually disappeared. A closer investigation of these hurricanes indicates that both traveled parallel to the New York/New Jersey coast, made their first landfall, and passed over eastern Long Island, New York, at the same location (East Hampton, NY). However, the storm surge and resurgence at NYH during the 1944 Hurricane were larger despite its lower intensity and maximum sustained wind speed (954 mb and 90 kt, respectively, compared with 955 mb and 100 kt in Hurricane Carol in 1954). This may be due to its path's closer proximity to the inner NYB (Figure 3).

Recently, more spatially resolved measurements show that resurgences tend to be far more prominent in the NYB than in other locations, even when a storm surge impacts the entire stretch of coastline in the study area (Figures 2b-h). NTRs exhibit spatial patterns that can be grouped based on visual similarities. For instance, stations in the same group recorded both storm surge and resurgence at nearly the same time, while some other stations recorded only storm surges and no accompanying resurgence. Thus, station groups can be: (1) Montauk to Nantucket Island, (2) Sandy Hook to Reynolds Channel, (3) Lewes to Atlantic City, and (4) Duck to Ocean City Inlet. Station group #2 records a clear storm surge with a secondary peak, markedly high at Sandy Hook, The Battery, and Great Kills Harbor inside NYH (Figure 2h).

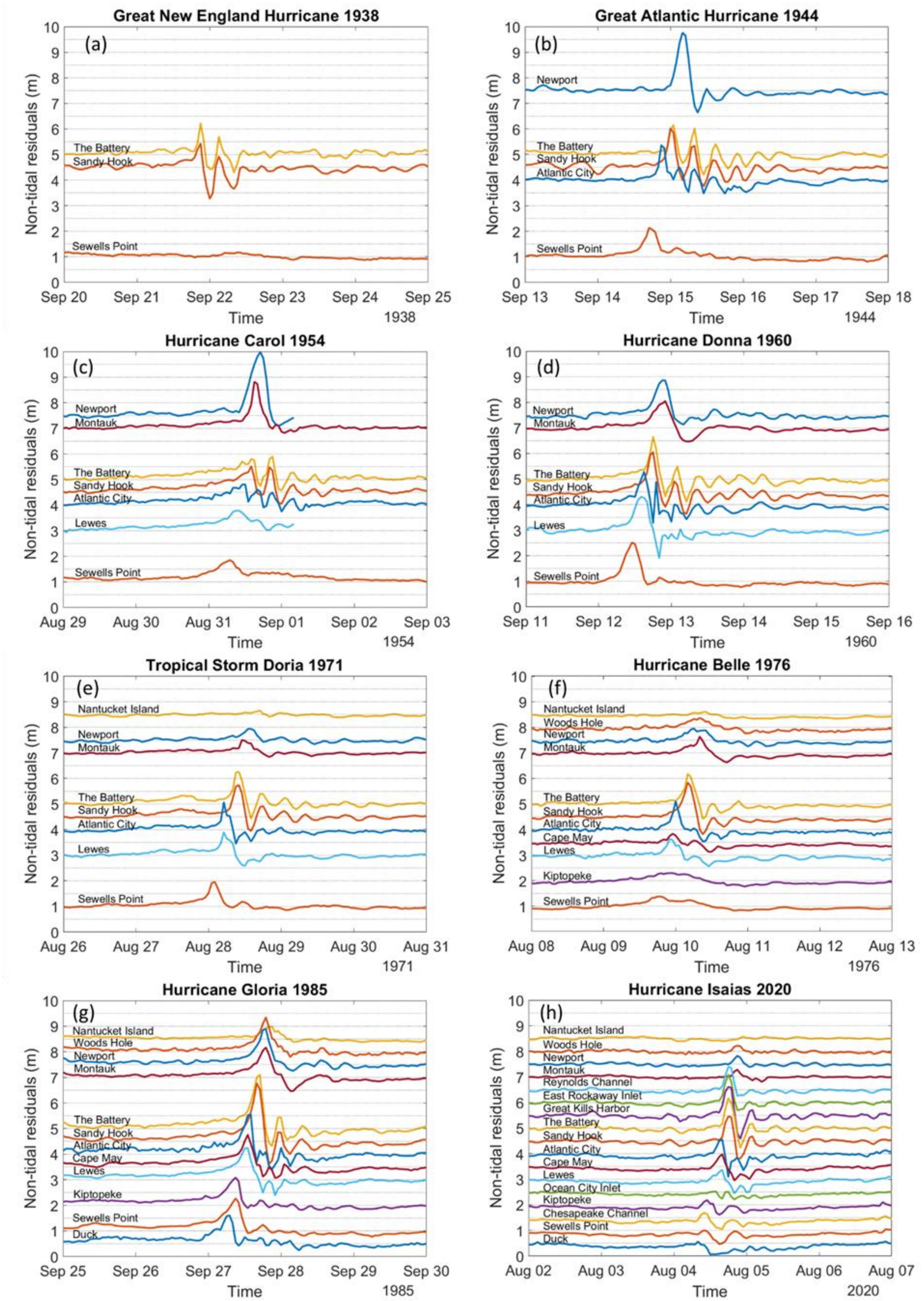


**Fig. 2.** Non-tidal residuals at selected tide gauges along the U.S. East Coast. Each successive time series is offset vertically by +0.5 m.

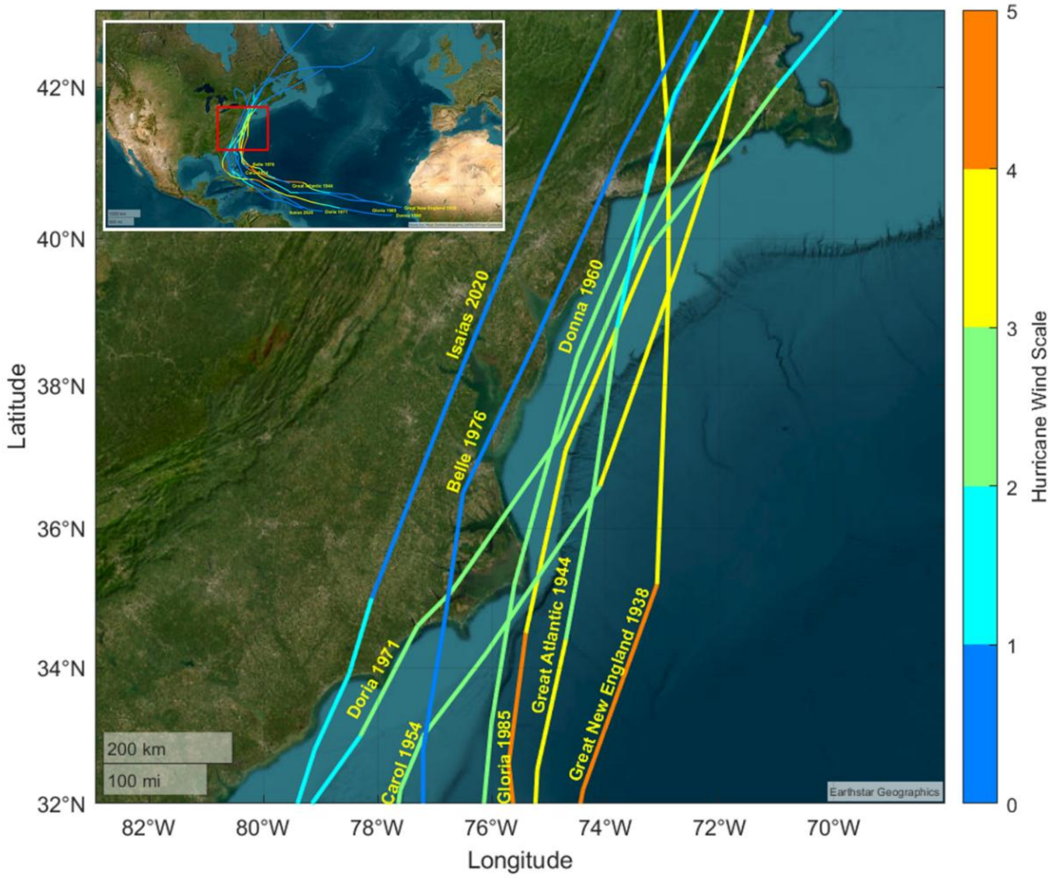


**Fig. 3.** Hurricane best track data from HURDAT (Landsea & Franklin, 2013), in which lines are drawn assuming the storm intensity remained the same over each 6 h segment.

### 3.2. Quantifying a resurgence: Example from 1944

The 1944 Great Atlantic Hurricane is an extreme example of the resurgence in water levels during historical hurricane events. Wind forcing from the southeast and east generated a surge of 1.17 m at NYH relative to the mean sea level. After the hurricane reached its peak intensity, the winds began shifting offshore, slowly changing direction from northeast to north and eventually to northwest (Figure 4a). Several distinct NTR peaks (resurgences) were still observed (Figure 4b). A secondary surge with a height of 1.25 m (trough to crest) was observed in the NTR at NYH. The first peak of NTR occurred at a time similar to the minimum barometric pressure; following this, five peaks in NTR occur periodically, with a period of approximately 7.0 h, and their heights gradually diminish after the initial peak.

The presence of a resurgence is clearly identified from the scalogram and distinguished from storm surges, for which energy is substantial but frequency is broadband. The wavelet transform analysis indicates the period of resurgence is ~7.0 h, and the resurgence wavelet amplitude is ~0.53 m (Figure 4c). Compared to the trough-to-crest resurgence height of 1.25 m (Figure 4b), the resurgence wavelet amplitude, which represents a time-integrated measure of amplitude, is less than half the resurgence height. Decay timescale of this resurgence is 20 h, as quantified by the e-folding time shown in Figure 4d. As expected, given the e-folding timescale, the complete observable duration of the resurgences (from September 15 to September 16, 1944, totaling 37 h) is nearly twice as long as the decay timescale.

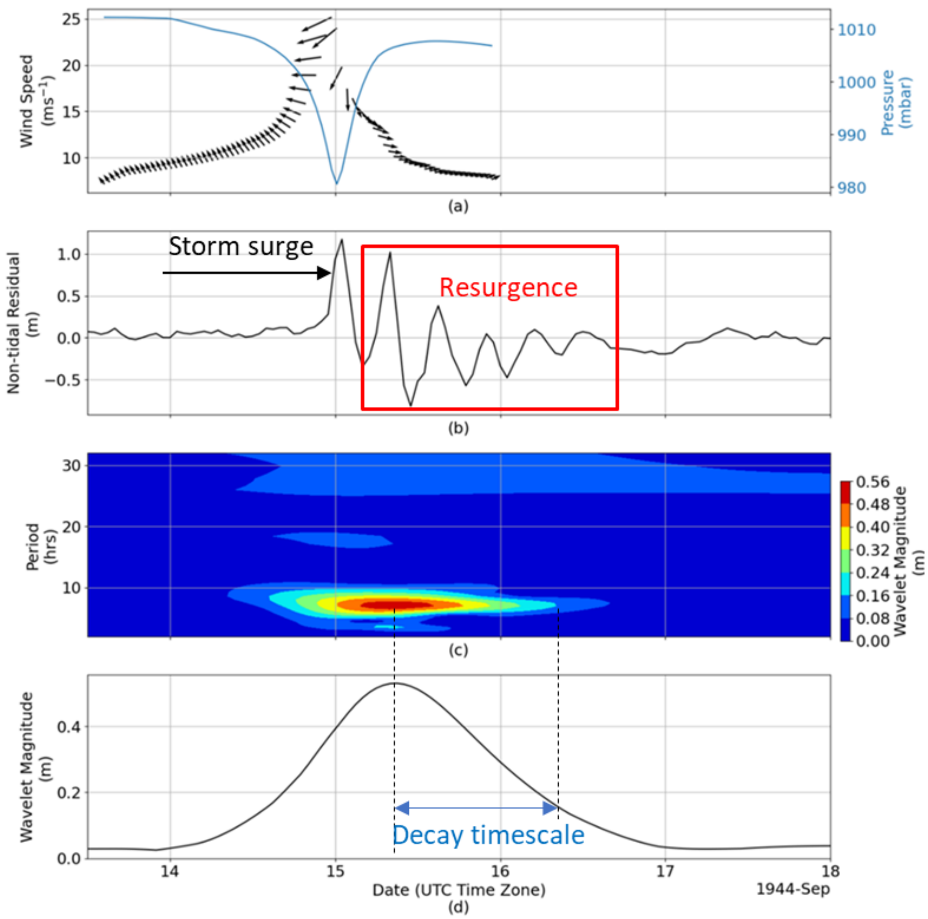


**Fig. 4.** Resurgence in the 1944 Great Atlantic Hurricane. (a) Pressure and wind speed during the Hurricane; (b) NTRs at NYH; (c) Wavelet scalogram; (d) Decay timescale.

### 3.3. Regression analysis

Based on the given list of criteria, 29 resurgence events out of 112 total TC events (26 %) in the NYB from 1860 to 2024 were identified (Figure 5a). Several relatively small resurgence events were recorded preceding 1930, whereas all larger resurgence wavelet amplitudes (0.4 - 0.5 m) were observed in the post-1930 period. Regression analysis reveals a statistically significant, moderate, positive linear correlation between storm surge and resurgence wavelet amplitude (*r = 0.47, p = 0.01; Figure 5b*), indicating that TCs producing larger storm surges are more likely to excite larger resurgences. Hurricane Sandy (2012) presents a notable outlier, with a resurgence amplitude of only 0.12 m, in contrast to its substantial storm surge of 2.8 m.

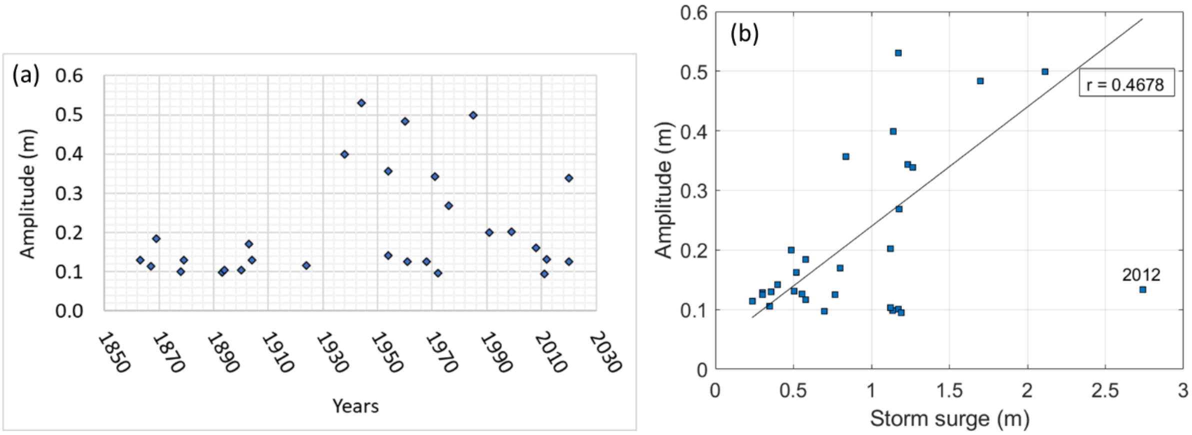


**Fig. 5.** (a) Resurgence wavelet amplitude from 1860 to 2024; (b) Robust regression for resurgence amplitude and storm surge. The year refers to the storm surge caused by Hurricane Sandy in 2012.

The correlation coefficients between storm parameters, including northward storm propagation speed ($V_{Nstorm}$), eastward storm propagation speed ($V_{Estorm}$), maximum sustained wind speed ($V_{max}$), approach angle ($\theta_{storm}$), and distance east of Sandy Hook ($D_{east}$), with resurgence characteristics (wavelet amplitude $R_{amp}$, period $R_T$, and decay timescale $R_{DT}$) are summarized in Table 2 (see Table S2 for p-values). Generally, $V_{Nstorm}$ and $V_{max}$ indicate a similar significant positive correlation with resurgence amplitude. Meanwhile, $V_{max}$ and $D_{east}$ show a negative relationship with the resurgence period. Only $V_{Nstorm}$ shows a significant negative correlation with the decay timescale.

**Table 2.** Correlation of NYH resurgence characteristics and storm parameters for 29 resurgence events from 1860 to 2024. Boldfacing indicates significant correlations ($p < 0.05$).

| ***Storm Parameters*** | ***Amplitude*** $R_{amp}$ | ***Period*** $R_T$ | ***Decay timescale*** $R_{DT}$ |
|---|---|---|---|
| $V_{Nstorm}$ *Northward storm speed* | **0.41** | -0.28 | **-0.55** |
| $V_{Estorm}$ *Eastward storm speed* | -0.15 | 0.17 | 0.03 |
| $V_{max}$ *Maximum sustained wind speed* | **0.41** | **-0.49** | -0.14 |
| $\theta_{storm}$ *Approach angle* | -0.03 | 0.06 | -0.10 |
| $D_{east}$ *Distance east of Sandy Hook* | 0.10 | **-0.38** | -0.29 |

Regression between $V_{Nstorm}$ and $R_{amp}$ indicates that fast TCs travelling northward can potentially generate significant resurgence events (Figure 6a). The plot shows that TCs having $V_{Nstorm} > 5$ m s$^{-1}$ can produce a resurgence in water levels. However, the most recurring resurgence events ($R_{amp} > 0.2$ m) typically occur when $V_{Nstorm} > 11$ m s$^{-1}$. This is supported by the statistically significant correlation between $V_{Nstorm}$ and $R_{amp}$ ($r = 0.41, p = 0.029$). In contrast, a significant negative correlation exists between $V_{Nstorm}$ and $R_{DT}$ ($r = -0.55, p = 0.002$), indicating that TCs moving northward at slower speeds tend to experience longer resurgence decay timescales (Figure 6b).

Similar to the results observed for $V_{Nstorm}$, a strong statistical relationship exists between $V_{max}$ and $R_{amp}$ ($r = 0.41, p = 0.03$) (Figure 6c and Table 2). In contrast, $V_{max}$ exhibits a significant negative correlation with $R_T$ ($r = -0.49, p = 0.01$) (Figure 6d and Table 2). $V_{max}$ is a widely used indicator of tropical cyclone intensity. In addition, $V_{max}$ exhibits a significant correlation with both $R_{amp}$ and $R_T$, which are the two key characteristics of a resurgence. Thus, it is chosen as the primary variable for the next phase of modeling simulations using idealized wind experiments.

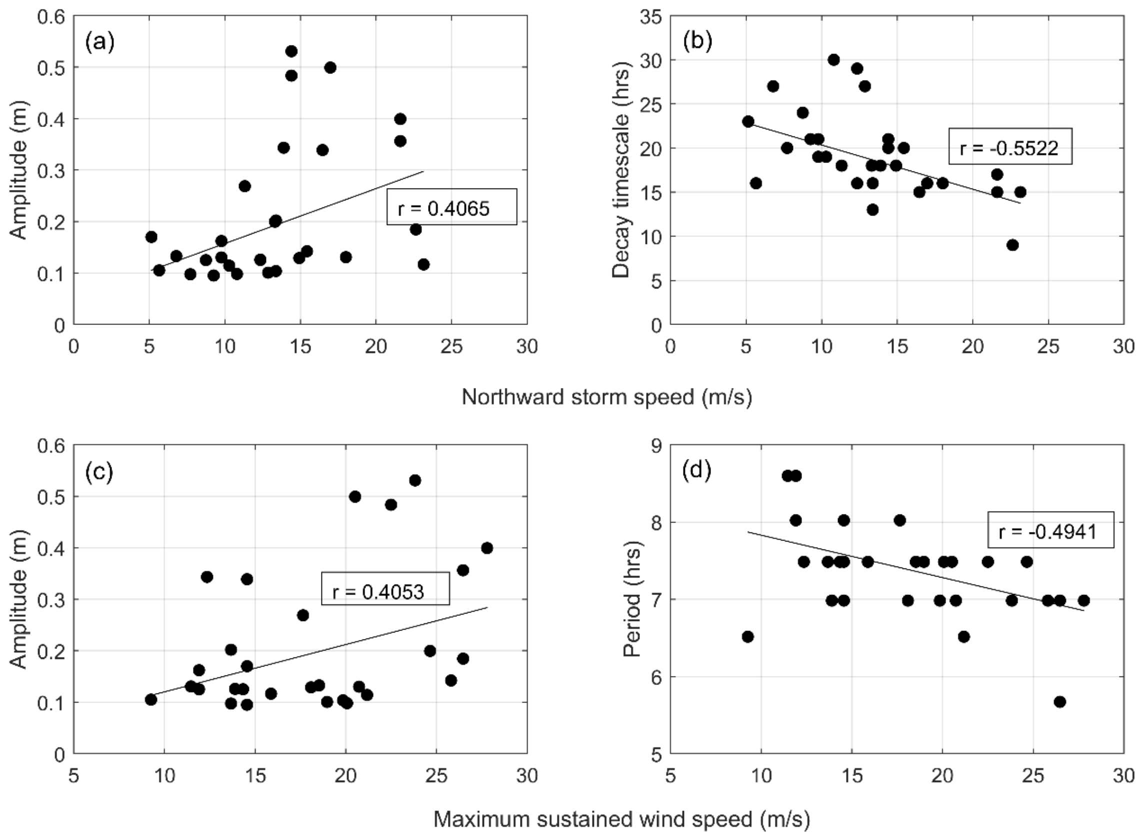


**Fig. 6.** Scatter plot with the corresponding regressions of (a) $R_{amp}$ vs. $V_{Nstorm}$; (b) $R_{DT}$ vs. $V_{Nstorm}$; (c) $R_{amp}$ vs. $V_{max}$; (d) $R_T$ vs. $V_{max}$.

The $D_{east}$ shows no significant correlation with $R_{amp}$, but a significant negative correlation with $R_T$ ($r = -0.38, p = 0.045$) (Supplemental Figure S1a). Our findings indicate that TCs with their central low pressure passing further to the east (e.g., hitting Long Island) are associated with shorter resurgence periods compared to those passing further to the west or inland. The largest resurgence events at NYH occurred when tropical cyclones passed near Sandy Hook, commonly between 110 km west and 130 km east of Sandy Hook. This indicates that resurgences tend to be small when storms are far away from the New Jersey coast (inland or offshore), similar to storm surges. Although less common, significant resurgence events may still be generated by storms traversing inland pathways, as opposed to offshore tracks. An upside-down T-shaped pattern is observed between $\theta_{storm}$ and $R_{amp}$, suggesting a narrow band of approach angles is needed for resurgences at the NYB. Supplemental Figure S1b indicates that TCs that produce a significant $R_{amp}$ have $\theta_{storm}$ from $10^o$ to $30^o$. The New Jersey coast angle is approximately $35^o$ in its southern half and $10^o$ in its northern half, averaging about $20^o$.

### 3.4. Results of the idealized wind model experiments

#### *3.4.1. Wind-forced water level response*

The largest magnitude of water level response is observed within the window of wind stress forcing within NYB at the time step corresponding to the end of the first day of simulation (Figure 7a). The modelled water levels across the study area differ between the control and non-Coriolis experiments. Specifically, the spatial distribution of water levels shows a peak water level of 1.59 m at Sandy Hook in the control experiment (Figure 7b), compared to a higher peak water level of 1.81 m in the non-Coriolis experiment (Figure 7c). Furthermore, when the Coriolis parameter is set to $f = 0$, the region experiencing high water levels expands both along-shelf and offshore. In contrast, in the control experiment, the offshore area north of NYB shows high water levels, whereas the southern area exhibits low water levels. This can be explained by the fact that Ekman flux convergence occurs on the right side of wind forcing in the Northern Hemisphere, and divergence occurs on the left side. However, despite the differences between the two experiments, both showed a spatially continuous rise in water levels from Montauk south to Lewes, while other areas remained near zero.

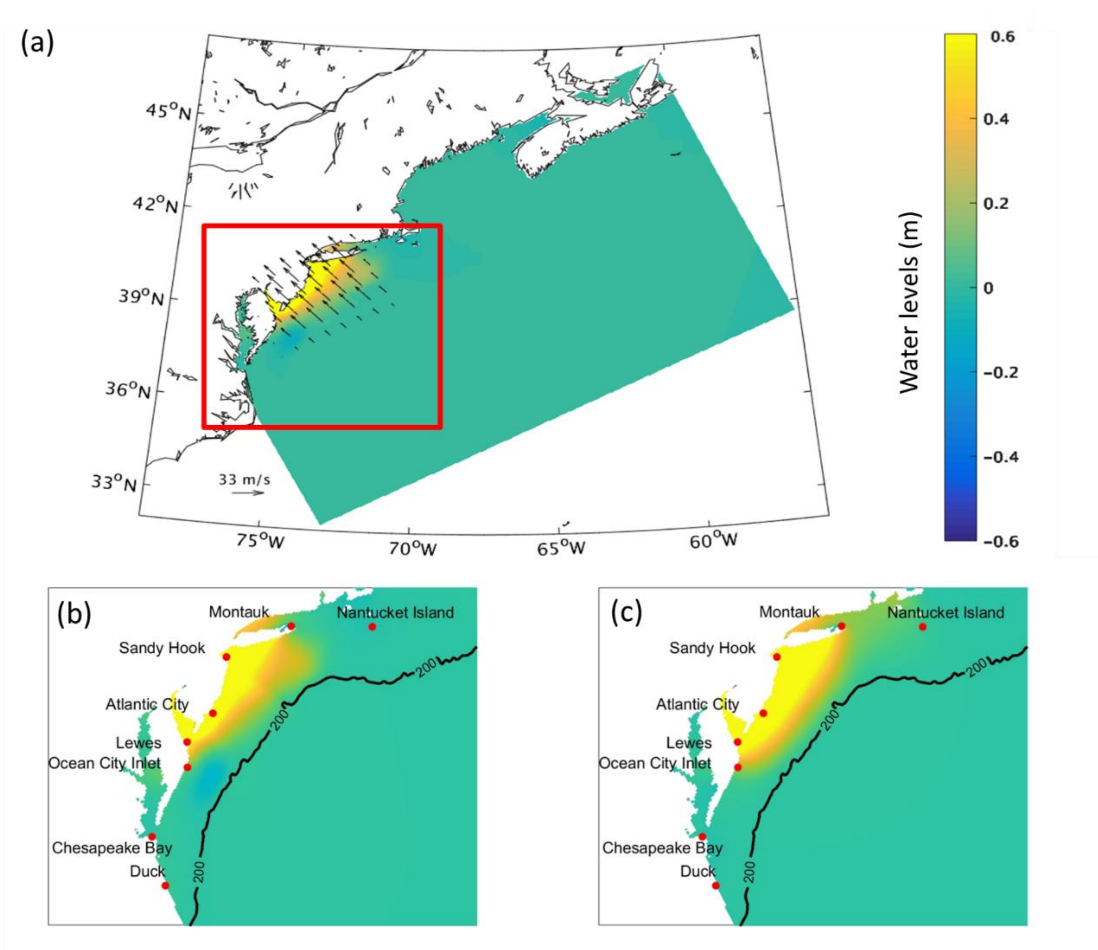


**Fig. 7.** Spatial distribution of water levels at the end of the first day (day 1.0) in the idealized wind forcing experiment. (a) Spatial extent of the onshore wind forcing within the full SNAP domain; Zoomed target study area with 200-m depth contour (b) in the control experiment and (c) in the non-Coriolis experiment.

#### *3.4.2. Free wave response after wind forcing stops*

For both simulations, the water level fluctuations after the wind stops at the end of day 1.0 can be considered as the "free wave" response, as there is no longer any external forcing acting on the water. The temporal and spatial evolution of the free wave response is illustrated from day 1.25 to approximately day 1.70 (corresponding to hour 30 to 41) in the control experiment (Figure 8) and the non-Coriolis experiment (Figure 9). In both cases, the maximum and minimum water levels are observed near the coast, particularly in the NYB. In contrast, water level variations are small near the shelf break and nearly unchanged throughout the adjacent deep ocean during the simulation period.

For the control simulation, the peaks and troughs in water level appear to move progressively down the coastline over time, corresponding to the movement represented by the blue and red arrows, respectively (see, e.g., the movement of the red arrows down-coast from day 1.25 to approximately day 1.41 (~4 h) in Figure 8). This oscillation continues, with peaks and troughs gradually diminishing until the water levels approach zero by the end of the simulation (day 5.0; not shown).

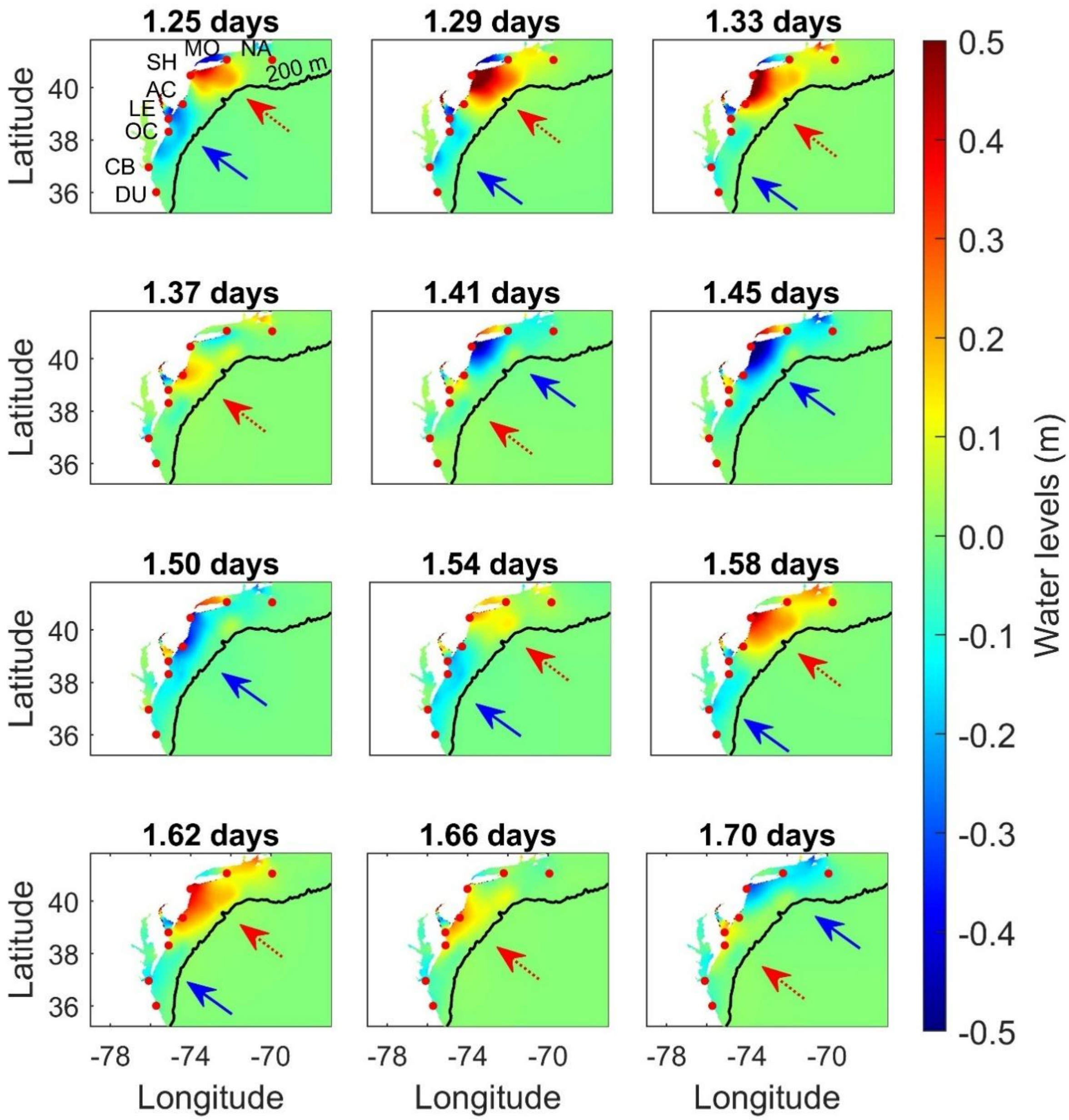


**Fig. 8.** Water level distribution from day 1.25 to approximately day 1.70 with an interval of one hour for the control idealized experiment. Abbreviation: NA - Nantucket Island, MA; MO - Montauk, NY; SH - Sandy Hook, NJ; AC - Atlantic City, NJ; LE - Lewes, DE; OC - Ocean City Inlet, MD; CB - Chesapeake Channel, VA; DU - Duck, NC. The black line shows the contour depth of 200 m at the shelf break. The red (dotted line) and blue (solid line) arrows point to the maximum and minimum water levels, respectively, and track the down-coast movement of highs and lows.

In the non-Coriolis experiment, water levels seem to rise and fall symmetrically on both sides of the NYB, consistent with a standing wave pattern rather than a propagating coastal wave. Similar to Figure 8, Figure 9 also presents a sequence of plots showing the spatial distribution of water levels across the study area from day 1.25 to approximately day 1.70 (hour 30 to ~41) of the simulation; however, no arrows are shown because the highs and lows do not move from NYB. In addition, it appears that more than one wave cycle is presented. The wave cycle begins around time t = 1.25 days, and after 7-8 h, it starts anew at time t = 1.54 days. A similar pattern is observed in Figure 8, where the water levels at NYH exhibit the highest variability and gradually decrease over time as the simulation progresses.

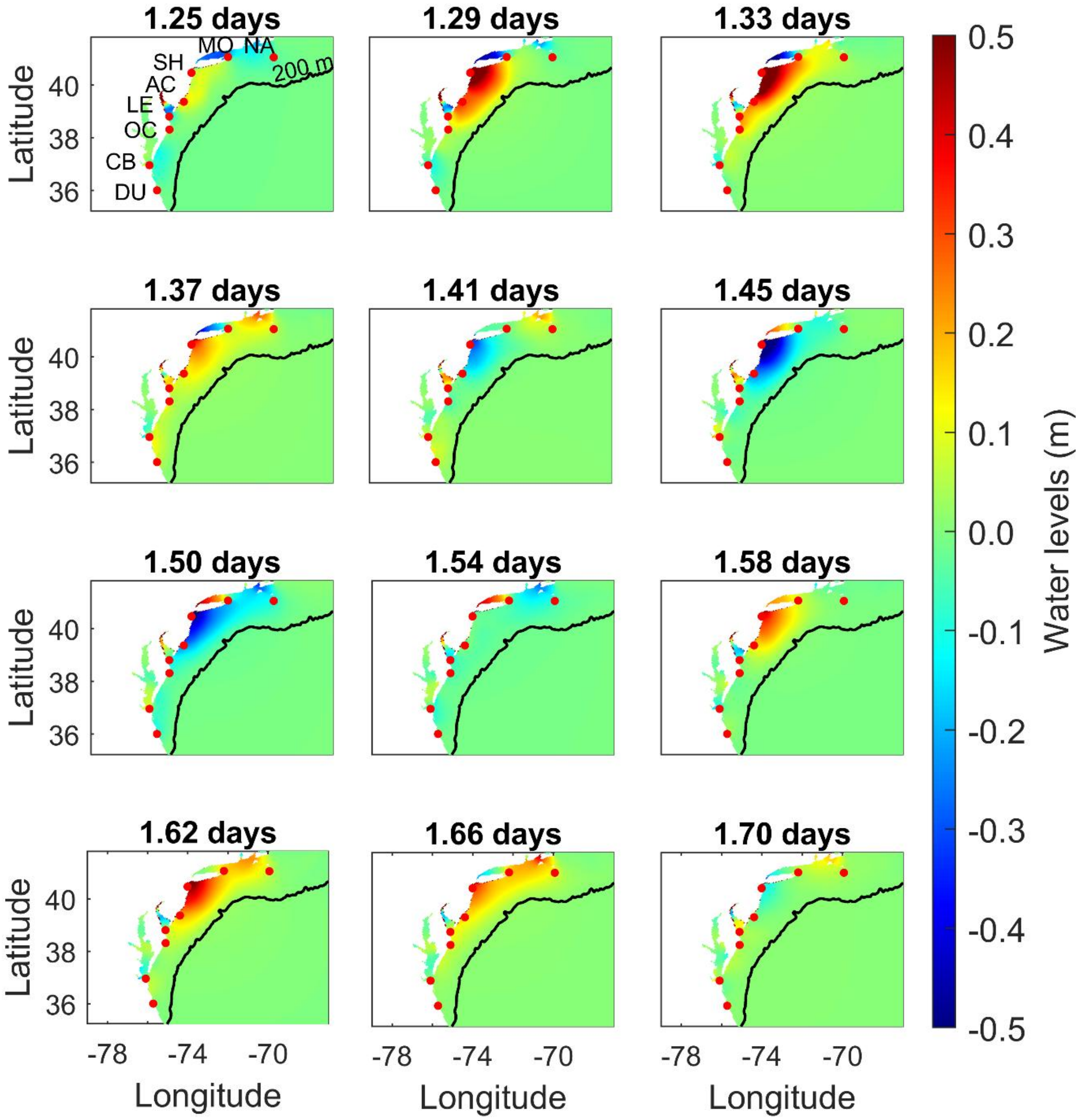


**Fig. 9.** Water level distribution from day 1.25 to approximately day 1.70, at one-hour intervals, for the non-Coriolis experiment. Abbreviation is the same as Figure 8. No arrows are shown because the highs and lows do not move from NYB.

The consistency of the modeled water levels and observed resurgence phenomenon is verified using a wavelet transform to quantify resurgence characteristics. In both cases of the control and non-Coriolis experiments, the wavelet scalogram reveals a local signal maximum with an amplitude of ~0.7 m and a period of 7.56 h (Supplemental Figure S2). The resurgence wavelet amplitude is higher than the maximum observed resurgence heights in historical TCs (e.g., 0.53 m in the Great Atlantic Hurricane of 1944). Still, this period matches observed resurgence periods (see the resurgence periods range in Figure 6d). The simulated resurgence decay timescales are 1.58 days in the control experiment and 1.54 days in the non-Coriolis experiment, indicating only a minimal difference between them. Both values are 1.5 to 2.5 times longer than those observed in historical events (Figure 6b). This extended duration observed in the idealized modeling experiments may result from the absence of tides and other storm- or ocean-related processes, which likely contribute to a reduced damping rate in the model.

#### *3.4.3. Modeled water level pattern on cross-shore and alongshore transects*

The cross-shore and alongshore transects exhibit rising and falling water levels over one cycle of approximately 7-8 h (e.g., Figures 8-10). The cross-shore transect (red asterisks, Figure 10a) runs from offshore of Sandy Hook past the shelf break to a location with a depth of 1,566 m (point 16). The alongshore transect (black dots, Figure 10a) follows the 50-m depth contour from Cape Cod to Cape Hatteras.

The temporal oscillation of water levels along the cross-shore transect in both experiments resembles the behavior of a standing wave, with a node at the shelf break and an antinode at the coast. Water level oscillations along the cross-shelf transect (Figures 10b and 10c) indicate that the highest and lowest water levels occur at the innermost location (near Sandy Hook) in both experiments. At the shelf break and further offshore in deeper waters, water levels exhibit small oscillations, remaining near zero at the deepest location throughout the simulation. This is clearer when tracing the hour-by-hour chronological sequence of water level lines in the experiments. Water levels along the transect reach their peak simultaneously at hour 2 in the control experiment (Figure 10b), and nearly simultaneously at hour 2 or 3 in the non-Coriolis experiment (Figure 10c). In both experiments, the water levels then decrease, reaching their minimum at hour 6, before rising again at hour 7. The water levels do not exhibit a perfectly idealized node at the shelf break, as a small oscillation remains. This likely reflects the realistic conditions in which the bathymetry does not drop off abruptly into an infinitely deep ocean, as assumed in an idealized seiche.

The behavior of a standing wave is also evident in the pattern of water level oscillations on the along-shelf transect. The maximum variation occurs in the apex of NYB with declining amplitude up- and down-coast. Here, Figures 10d and 10e show that the entire NYB study area (alongshore points 10 to 30) undergoes nearly synchronous fluctuations in both experiments. The maximum and minimum water levels are typically observed offshore of Sandy Hook (point 21). In the control experiment, there is motion from the right-hand side to the left-hand side of the NYB (north to south) between day 1.25 (hour 1) and day 1.37 (hour 4) (Figure 10d). Despite this southward movement, water levels decrease with distance and become very small beyond Delaware Bay, while the oscillation remains centered off Sandy Hook during each cycle. Meanwhile, no alongshore propagation is observed in the non-Coriolis experiment (Figure 10e).

Nevertheless, in both experiments, persistent small water-level oscillations are observed eastward from Montauk (MO) to Nantucket (NA).

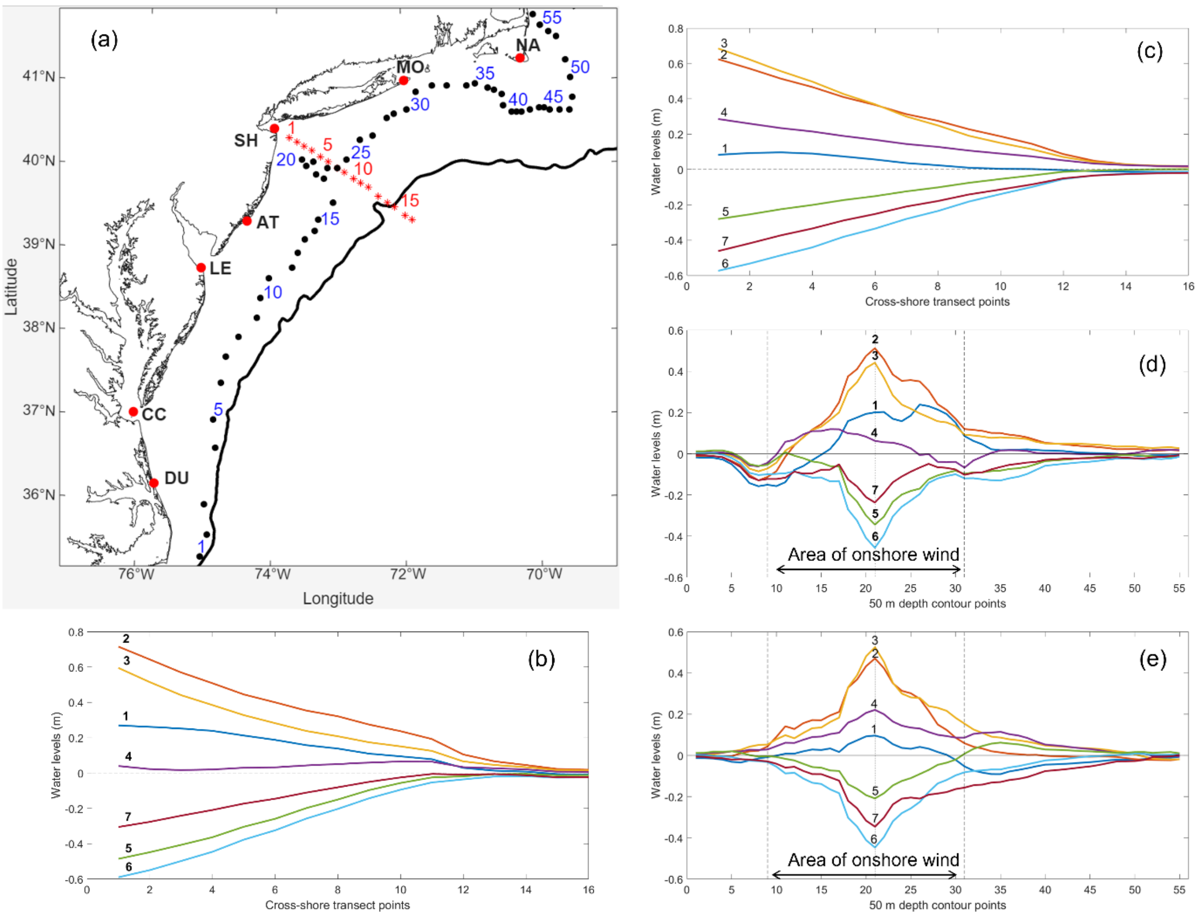


**Fig. 10.** (a) Our study domain shows the cross-shore transect and alongshore transect represented by red asterisks and black points, respectively. Water level changes from hour 1 to 7 (day 1.25 - 1.5) as shown in numbers on the cross-shore and alongshore transects in the (b and d, respectively) control experiment, and (c and e, respectively) non-Coriolis experiments. Dashed vertical lines in (d and e) indicate the wind forcing window (points 9 to 31).

Strong evidence of a standing wave centered at NYB is shown in both Hovmöller diagrams (control and non-Coriolis; Figures 11 a and b, respectively). In both experiments, the cycle of water-level oscillations repeats with gradual decay through the end of the simulation (day 5). The largest amplitude occurs from along-isobath distance 400-500 km (alongshore points 20-23), which is the middle of NYB. In the control experiment, there is a slight counterclockwise inclination of the wave crests (red) and troughs (blue), reflecting a predominant alongshore movement from the north (large along-isobath distance) to the south (small along-isobath distance). There is also temporal variation and some irregularity, likely attributable to the complexity of the coastline and shelf bathymetry. The non-Coriolis case has temporal and spatial variations in crest and trough angles, but they generally exhibit more of a clockwise rotation relative to the control experiment. A detailed quantification of time lags is presented in the next section on cross-correlation analysis results.

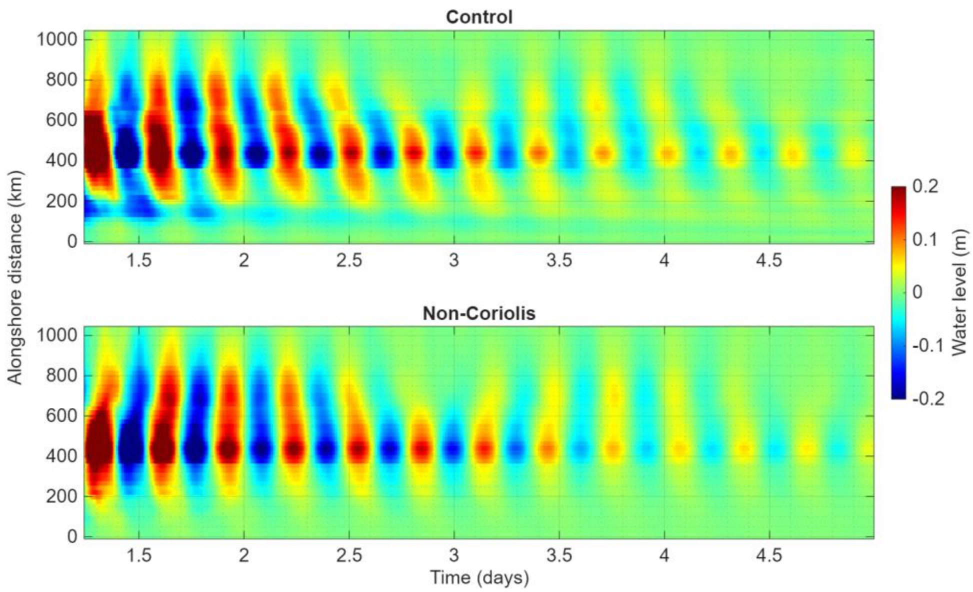


**Fig. 11.** Hovmöller diagram of water level anomaly versus time and distance along the 50-m depth isobath in the (a) control experiment and (b) non-Coriolis experiment

### *3.4.4. Cross-correlation analysis results*

Maximum cross-correlation values and their corresponding time lags relative to Sandy Hook are used to examine the time-integrated wave motions across the study area. For time 1.25 to 5.0 in the control experiment, offshore Nantucket and Montauk lead Sandy Hook by 0.67 h and 0.50 h, respectively. Meanwhile, Atlantic City and Ocean City Inlet lag by 1.0 h and 1.67 h, respectively (Figure 12a). This indicates the presence of an alongshore component in wave propagation, spanning the region from Nantucket to Sandy Hook and Ocean City Inlet. Further south along the continental shelf, the time lag shifts to positive values (e.g., greater than 4 h), potentially influenced by the internal dynamics of Chesapeake Bay. However, without the Coriolis force, the time lags are near zero within NYB and reach values of -0.50 h and -0.33 h at Nantucket and Ocean City, respectively, suggesting an outward spreading from Sandy Hook (Figure 12c).

The Hovmöller diagrams (Figure 11) indicate that there is some time dependence to the wave motions, with differences in the earlier cycles of free wave propagation shown (day 1.25-2.00) relative to the remainder of the simulation (day 2.0-5.0). Repeating the cross-correlation analysis for each period, we find the control results are the same for time lags from Sandy Hook to Ocean City (1.67 h for either time period). However, they are smaller for Nantucket to Sandy Hook in the earlier time period (0.33 h) relative to the later time period (1.83 h). That is, the earlier period shows a near-simultaneous wave arrival at Nantucket and Sandy Hook, in contrast to the period from day 2.0 onward.

Strong cross-shelf correlations in both experiments highlight synchronized water level behavior within the NYB. However, for the control run, a reduced correlation of ~0.6 in the outer shelf region (Figure 12b) suggests that additional dynamical processes may significantly contribute to the variability of water levels on the outer shelf. The constancy of the time lag in the cross-shore dimension in the NYB in the control experiment (Figure 12a) and for all shelf regions in the non-Coriolis experiment (Figure 12c) suggests the existence of a standing wave pattern across the shelf, consistent with the findings presented in Section 3.4.3. In addition, although the signal propagates downcoast, the reduced correlation of water levels southward of Ocean City and particularly near Chesapeake Bay reflects a phase shift as the disturbance interacts with the complex coastal geometry. In the non-Coriolis experiment, propagation is both up-coast and down-coast and remains coherent with little phase disruption. In contrast, when the Coriolis force is included (control experiment), interactions with Delaware Bay and Chesapeake Bay introduce phase modifications that reduce correlation without inhibiting the general trend of downcoast propagation from Nantucket to Sandy Hook and southward to Ocean City.

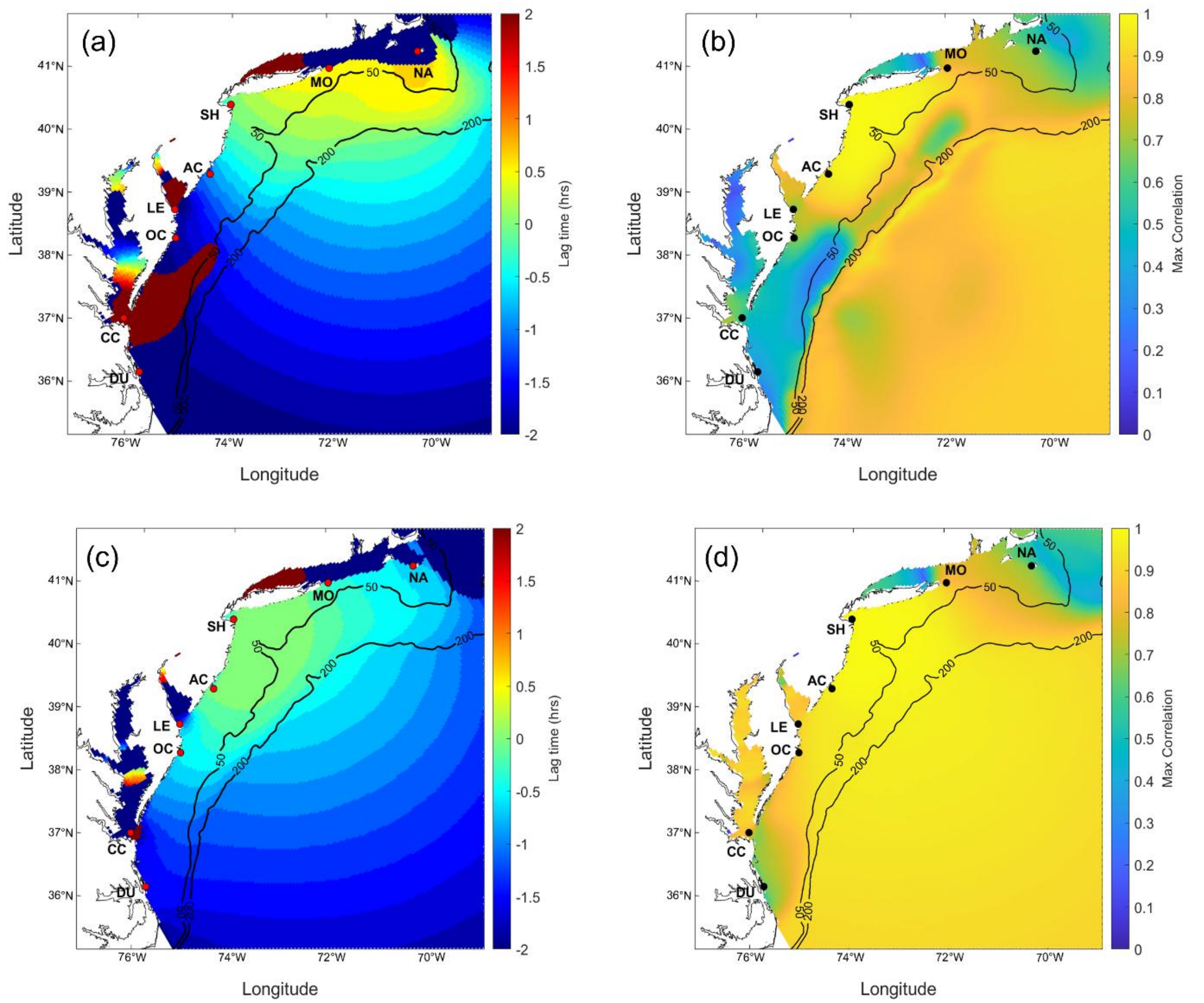


**Fig. 12.** Cross-correlation analysis of water levels between Sandy Hook and the study area from day 1.25 to 5.0. Panels (a) and (b) show the time lag and maximum correlation, respectively, for the control experiment. Panels (c) and (d) present the corresponding results for the non-Coriolis experiment.

## 4. Discussion

Water level resurgences are a fundamental yet insufficiently understood aspect of storm-driven NTR that can be of a similar magnitude to storm surge, particularly in the New York Bight region (e.g., Figures 2 & 4). Although interpretations of edge waves and shelf seiches have been proposed for resurgences in the NYB, a definitive understanding of the mechanisms driving these events has remained elusive. This research applies novel methods, including wavelet analysis and numerical simulations, to systematically detect, quantify, and investigate resurgences and their underlying mechanisms. Results (Figures 8-11) suggest that resurgences between Montauk and Cape May are predominantly a cross-shelf seiche, a standing wave that is amplified and trapped in the NYB. In the sections that follow, we examine the evidence supporting seiche behavior (Section 4.1). The secondary along-coast movement is discussed in light of its disappearance in the idealized modelling experiment excluding the Coriolis force (Section 4.2). Lastly, we examine the relationships between resurgence characteristics and tropical cyclone parameters (Section 4.3).

### 4.1. Primary mechanism of NYB resurgences: wind-driven cross-shelf seiches

Several lines of evidence support the conclusion that the primary mechanism of resurgence at the NYB is a wind-induced continental shelf seiche. Here, mainly onshore winds during a storm increase the water level at the coast, and as the storm propagates away, the winds decrease. This sets up a seiche with a node generally at the shelf break and an anti-node at the coast. First, our idealized onshore wind simulations, excluding pressure disturbances, replicate the resurgence pattern in the NYB. This finding contradicts the conclusion of Munk et al. (1956). They attributed the resurgence to low-pressure systems propagating along the coast, which generate coastal edge waves trapped by refraction, with amplitudes on the order of the inverted barometer effect. Instead, our results support the hypothesis of Redfield and Miller (1957) that resurgence phenomena in the NYB exhibit characteristics of seiche oscillations. Identifying a 7.56-hour oscillation in the idealized wind forcing simulations, consistent with the observed resurgence, provides further evidence that the wind-driven storm surge and its abrupt release are the drivers of the phenomenon. Second, the modeled water-level variations along the cross-shelf and along-shelf transects (Figure 10) show that the entire NYB undergoes nearly synchronous fluctuations, indicative of a localized standing wave. Critically, these free oscillations remain trapped in the NYB for several days after all forcing has ceased. These results are further supported by the analysis of the Hovmöller diagram in Figure 11. Third, although the cross-correlation analysis indicates that some down coast wave propagation, the water level variations down the coast, in the south (Figure 10d points 1-10) are much smaller than those at the apex of the NYB, where the amplitudes are maximal. This suggests that most of the energy is trapped within the NYB and behaves like a standing wave (seiche) with only a small fraction of energy leaking into along-coast propagating waves. Lastly, the non-Coriolis experiment reveals both that the Coriolis effect is necessary for the alongshore wave progression and, most crucially, that the primary oscillation remains of the same amplitude (0.701 m in the control experiment and 0.697 m in the non-Coriolis experiment) and of the same period (7.56 h) when this alongshore movement is absent (see Supplemental Figure S2).

In both numerical experiments, the concave NYB coastal geometry appears to both amplify and trap the seiche, as was observed with historical TCs (Figure 2). The idealized wind forcing simulation extends from Montauk to Ocean City Inlet, but the peak of resurgence remains stationary at the apex of the NYB (Figure 10c) throughout the remainder of the 5-day simulation. A concave coastal geometry, such as the NYB, is known to amplify storm surges (Deb et al., 2024; Gurumurthy et al., 2019; Harris, 1957; Redfield & Miller, 1957) and this research extends that effect to include the trapping and amplification of shelf seiches. Similarly, semidiurnal lunar (M2) tidal amplitudes are amplified by 17% between Atlantic City (0.58 m) and Sandy Hook (0.68 m).

Along-coast transects reveal that energy remains trapped at the NYB in both experiments, with amplitudes considerably larger at the NYB compared to surrounding locations. For example, in the control simulation during the period shown in Figure 8, the maximum water level at SH is 1.03 m, while at Atlantic City it is 0.34 m, a factor of ~3 smaller. At Montauk and Lewes, the maximum levels are 0.20 m and 0.26 m, respectively, and at Nantucket Island and Ocean City Inlet, they are 0.19 m and 0.17 m, respectively, a factor of ~5 smaller than at SH.

Two additional idealized wind experiments were conducted to investigate the sensitivity of these results to wind direction. Simulations with an east or south wind led to similarly persistent oscillations that were smaller, but nevertheless much larger at Sandy Hook than down- or up-coast at Ocean City or Cape Cod. These results suggest that other wind directions can still trigger seiching at NYB and the along-coast wave movement under this forcing remains relatively small. Other research has shown that seiches can be triggered by extratropical cyclones (Ozsoy et al., 2016; Pasquet et al., 2013) which often have longer-duration, alongshore winds, and these results suggest that extratropical cyclone-driven seiches could also occur at NYB.

Cross-shelf seiches are difficult to identify visually in comparison to along-shelf wave propagation (e.g., from Figure 9) and require deeper investigation because the cancellation of incident and phase-shifted reflecting components of the wave leads to nearly zero amplitude at the shelf break (George et al., 2020; Howarth, 1979). To illustrate this concept in a simplified manner, we synthesized two opposing waves on a continental shelf: one propagating shoreward and the other seaward, resulting in the black line in Figure 13. The reflection at the coast is a mirrored reflection (zero-degree phase shift) and thus the incoming wave and outgoing wave are matched and amplitude doubled, whereas we assume that the reflection at the shelf break is an approximately 180-degree phase-shifted (negative) wave reflection, causing the two waves to cancel. The resulting standing wave exhibits maximum amplitude at the coast, where the oscillations are amplified, and approaches zero amplitude in the deep ocean, consistent with the water-level variations observed along the cross-shore transect in Figure 10. This agreement highlights the physical relevance of the standing-wave interpretation. Such behavior is identical to idealized shelf (or bay) quarter-wave tidal resonance, with a node at the shelf break and an antinode at the coast. Storm-driven seiches in the New York Bight only differ from quarter-wave tidally resonant systems (e.g., the Gulf of Maine) in that there is no periodic forcing; no additional energy is added to the trapped wave with every tidal cycle. Moreover, understanding these storm-driven seiches is complementary to understanding quarter-wave tidally resonant systems, due to the similar coastal and shelf-break reflections and trapping processes.

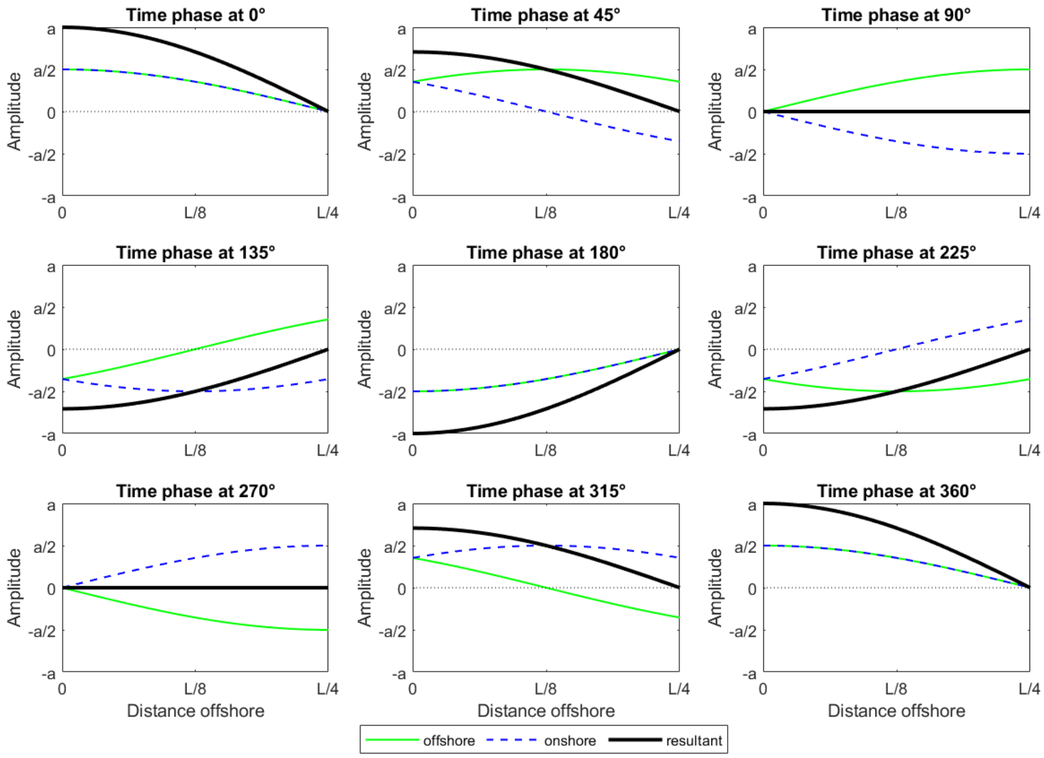


**Fig. 13.** Illustration of the kinematics of a shelf seiche. A sinusoidal cross-shelf wave form is assumed, with perfect coastal reflection at $X = 0$ and negative reflection (180° phase shift) at $X = L/4$, where L is the seiche wavelength and $L/4$ corresponds to the continental shelf width. The amplitude of the offshore and onshore waves is "a/2", while the maximum amplitude of the resultant wave is "a". An animation is included in Supplemental Figure S3.

### 4.2. Secondary along-shelf movement

The observed southward phase progression in the control experiment is consistent with the behavior of Kelvin waves. A Kelvin wave is a type of free wave strongly influenced by the Coriolis force, propagating unidirectionally along a boundary with the coast on its right in the Northern Hemisphere (Cushman-Roisin & Beckers, 2011; Stewart, 2008). This behavior is clearly visible in the pattern of NTR propagation along the coast (Figure 8) and in the shift leftward from hour 1 to 4 in the along-shelf transect (Figure 10c). Conversely, in the experiment without the Coriolis effect, the water level oscillates synchronously within the NYB, with phase lags on both sides indicating that the main locus of trapped wave energy is at the center. The potential influence of the Coriolis effect is supported by a computed Rossby number ($R_o$) of ~0.006, far below 1. Here, $R_o=U/Lf$ (Cushman-Roisin & Beckers, 2011), where modeled water speeds ($U$) on the shelf are $O(0.1)$ m s$^{-1}$, shelf width ($L$) is 190000 m, and Coriolis parameter ($f$) at this latitude is 0.000094. However, the Rossby radius of curvature (Cushman-Roisin & Beckers, 2011) is *sqrt(gh)/f* ~240 km, where the mean shelf depth ($h$) is ~50 m, supporting only a weak tendency of the wave energy to turn down the coast.

Edge waves are commonly observed in coastal environments, where the bathymetric slope serves as the primary mechanism for trapping wave energy through refraction, as described in the formulations of Munk et al. (1956). Edge waves are not rotationally controlled, whereas on the continental shelf, the Coriolis effect becomes increasingly dominant at larger spatial and temporal scales. As geostrophic balance plays a significant role in governing oceanic water movement, Kelvin waves become more relevant. In addition, according to Pattiaratchi et al. (2022), edge waves can propagate both up- and down-shelf, which is not observed in our control simulation.

Lastly, the wave speed inferred from the cross-correlation analysis is inconsistent with the behavior of an edge wave. Supplemental Figure S4b illustrates the time lags corresponding to the highest cross-correlation values, referenced to the northernmost tide gauge at Nantucket Island, with an estimated speed of 66.7 m $s^{-1}$ for wave phase propagation from Nantucket Island to Ocean City Inlet (see their location in Supplemental Figure S4a). For comparison, the theoretical speed of an edge wave given by the dispersion relation of $gT(\sin \beta)/2\pi$ used by Munk et al. (1956) is 18 m $s^{-1}$, where $\beta$ is beach inclination or slope of the bathymetry, $g$ is the gravitational acceleration, and $T$ is the wave period. We thus conclude that the large-scale alongshore movement in the control experiment is better described by Kelvin waves, rather than by classical edge wave behavior.

### 4.3. Resurgence characteristics associated with Tropical Cyclone parameters

Regression analysis identifies two storm-related parameters with significant correlations to resurgence amplitude: northward translation speed ($r = 0.41$) and maximum sustained wind speed ($r = 0.41$), in addition to the strong correlation with storm surge ($r = 0.47$). Early theoretical work by Munk et al. (1956) and Greenspan (1956) concluded that resurgences occur with rapidly moving tropical cyclones traveling parallel to a straight coastline, emphasizing the importance of the storm track and speed. Our study, drawing on an extensive historical dataset, both corroborates these seminal insights and extends them by quantifying the relative influence of these storm characteristics on the formation of resurgence. It also offers a few additional clues for further, more detailed research.

Firstly, our results suggest that the northward storm speed plays a crucial role in the NYB resurgence wavelet amplitude, with larger (>20 cm) amplitudes only observed for fast-moving (>11 m $s^{-1}$) tropical cyclones. Reviewing the large resurgences observed by Munk et al. (1956) and Greenspan (1956), northward storm propagation speeds ranged from 14.3 m $s^{-1}$ to 15.2 m $s^{-1}$. However, TCs with relatively slow storm speeds were able to produce smaller resurgence events. For example, the New Jersey Hurricane of 1903, with a storm speed of 5.3 m $s^{-1}$ approaching the NYB, corresponding to a northward speed of ~5.0 m $s^{-1}$, generated a resurgence amplitude of 0.17 m at NYH. Another case is Hurricane Sandy, with a storm speed of ~8.0 m $s^{-1}$, corresponding to a northward speed of 6.8 m $s^{-1}$ when making landfall near Brigantine, New Jersey, as a tropical storm, producing a resurgence wavelet amplitude of 0.13 m.

Secondly, significant resurgence amplitudes are observed only at wind speeds exceeding 12 m $s^{-1}$. Wind speed shows a positive linear correlation with resurgence amplitude and a negative correlation with resurgence period. Specifically, TCs associated with weaker wind speeds tend to produce resurgences with longer periods, whereas stronger wind speeds are linked to shorter resurgence periods. Meanwhile, the decay timescale of resurgences is linked to the northward storm propagation speed. Fast-moving storms, such as the 1938 Long Island Express

Hurricane, likely generate storm surges with limited spatial extent relative to the large scale of the NYB, thus less overall scale and energy for the trapped seiche, resulting in faster decay.

Our results show that TCs moving parallel to the New Jersey coast can cause significant sea level resurgences, as observed by Greenspan (1956). However, some tropical cyclones, such as Hurricane Two in 1904 and Hurricane Zeta in 2020, whose paths travelled from inland toward the sea, still generated a resurgence. In addition, the significant negative linear correlation between $R_T$ vs $D_{east}$ (Table 2, Supplemental Figure S1a) suggests that TCs further offshore in the NYB produce resurgence events with shorter periods than those passing close to the New Jersey coast or inland to the west. This could arise if the narrower southern New England continental shelf (south of Newport, Nantucket, and Cape Cod) results in shorter-period seiches.

## 5. Summary and Conclusions

This research investigates the historical occurrences and mechanisms of water level resurgences in the NYB associated with tropical cyclones. Through the analysis of historical water level observations from 17 tide gauges distributed along the U.S. Mid-Atlantic Bight coast, we demonstrate that the NYH area exhibits significantly elevated resurgence magnitudes compared to other sites across the study region. To examine the mechanism of resurgence, we examine water level data for NYH during 112 TC events from 1860 to 2024. Wavelet analysis is applied to detect resurgences and quantify their characteristics. Resurgence wavelet amplitudes range from 0.10-0.53 m, periods vary from 5.7-8.6 h, and e-folding decay timescales range from 9-30 h. Based on linear regression analysis, we find significant correlations between resurgence amplitude and initial storm surge, as well as both maximum sustained wind speed and northward storm speed, suggesting that these forcing variables are prerequisites for a significant resurgence event.

The observations and regression analysis results motivate experiments with idealized onshore wind forcing that ramps up and then abruptly shuts off, mimicking the rapid approach and passage of a tropical cyclone. These simulations reproduce resurgences both with and without the Coriolis effect, with the primary difference being the absence of southward water propagation along the coast when the Coriolis force is removed. Model results display a clear across-shelf standing wave pattern, indicative of a shelf seiche. Transect analyses reveal significant energy trapping and amplification at the NYB, with water level amplitudes substantially higher than those in the surrounding regions. The Coriolis forcing modifies the response, resulting in spatial time lags and a southerly alongshore movement. We conclude that Kelvin waves are a secondary mechanism that may arise under specific conditions, leading to energy leakage from the seiche down the coast, and thereby modestly influencing their directionality and spatial structure.

Given the unforeseen and potentially hazardous nature of these seiches, which occur hours to days after the passage of a tropical cyclone and have a magnitude often greater than half that of the initial storm surge, more research is needed. Through their superposition and interaction with tides, these continental shelf seiches can prolong the duration of the acute phase of a storm event. Public safety messaging on hazards coming after a storm passes may be a challenge, and the range of hazards could include strong currents, flooding, or ship grounding if extrema in seiche water levels coincide with extrema in tides, as well as severe coastal erosion as seiche highs coincide with large post-storm swells on an already eroded coast. In ongoing research, we are assessing the prevalence of these events across the United States Gulf and East Coasts, their total number of historical occurrences regardless of storm forcing conditions, and a wide range of potential resulting hazards.

## Appendix A. Supplementary material

Supplementary material associated with this article is provided as a separate file submitted with the manuscript. This includes additional figures and tables supporting the results presented in the main text.

## Data availability

All datasets used in this study are publicly available data, including tide gauge data from the National Oceanographic and Atmospheric Administration (NOAA) (https://tidesandcurrents.noaa.gov/) and the United States Geological Survey (USGS) (https://www.usgs.gov/). In the case of the composite "New York Harbor" dataset from 1860 to 2024, the data for the noted individual stations are available in Haigh et al. (2023) and the GESLA-4 dataset (https://gesla787883612.wordpress.com/).

## Acknowledgements

The lead authors would like to thank Johannes Westerink for providing initial guidance on the topic of shelf seiches.

## Funding

The research was funded by the National Science Foundation PREEVENTS program (award 1855037), the NOAA Climate Program Office's Climate Adaptation Partnerships (CAP, formerly RISA) program (award NA21OAR4310313), and a Provost's Doctoral Fellowship from the Stevens Institute of Technology. SAT was funded in part by the Strategic Environmental Research and Development Program, contract W912HQ24C0020.

## Author contributions

TTT: Formal analysis, Investigation, Methodology, Visualization, Writing – original draft, Writing – review & editing

PO: Conceptualization, Funding acquisition, Methodology, Project Administration, Supervision, Validation, Visualization, Writing – review & editing

SAT: Conceptualization, Methodology, Data curation, Writing – review & editing

MA: Methodology, Visualization, Writing – review & editing

CP: Conceptualization, Methodology, Writing – review & editing

## Declaration of competing interests

The authors declare that they have no known competing financial interests or personal relationships that could have appeared to influence the work reported in this paper.

## References


Ayyad, M., Orton, P. M., El Safty, H., Chen, Z., & Hajj, M. R. (2022). Ensemble forecast for storm tide and resurgence from Tropical Cyclone Isaias. *Weather and Climate Extremes*, *38*, 100504. https://doi.org/10.1016/j.wace.2022.100504

Blumberg, A. F., & Georgas, N. (2008). Quantifying Uncertainty in Estuarine and Coastal Ocean Circulation Modeling. *Journal of Hydraulic Engineering*, *134*(4), 403-415. https://doi.org/10.1061/(ASCE)0733-9429(2008)134:4(403)

Cushman-Roisin, B., & Beckers, J.-M. (2011). *Introduction to geophysical fluid dynamics: physical and numerical aspects* (Vol. 101). Academic press.

Cushman-Roisin, B., & Beckers, J.-M. (2011). *Introduction to Geophysical Fluid Dynamics: Physical and Numerical Aspects*. Elsevier Science. https://books.google.com/books?id=3KS8sD5ky9kC

Deb, M., Benedict, J. J., Sun, N., Yang, Z., Hetland, R. D., Judi, D., & Wang, T. (2024). Estuarine hurricane wind can intensify surge-dominated extreme water level in shallow and converging coastal systems. *Nat. Hazards Earth Syst. Sci.*, *24*(7), 2461-2479. https://doi.org/10.5194/nhess-24-2461-2024

Devlin, A. T., Jay, D. A., Talke, S. A., & Pan, J. (2023). Global water level variability observed after the Hunga Tonga-Hunga Ha'apai volcanic tsunami of 2022. *Ocean Sci.*, *19*(2), 517-534. https://doi.org/10.5194/os-19-517-2023

Dodet, G., Melet, A., Ardhuin, F., Bertin, X., Idier, D., & Almar, R. (2019). The Contribution of Wind-Generated Waves to Coastal Sea-Level Changes. *Surveys in Geophysics*, *40*(6), 1563-1601. https://doi.org/10.1007/s10712-019-09557-5

Dusek, G., DiVeglio, C., Licate, L., Heilman, L., Kirk, K., Paternostro, C., & Miller, A. (2019). A Meteotsunami Climatology along the U.S. East Coast. *Bulletin of the American Meteorological Society*, *100*(7), 1329-1345. https://doi.org/10.1175/BAMS-D-18-0206.1

Eliot, M. (2010). Influence of interannual tidal modulation on coastal flooding along the Western Australian coast. *Journal of Geophysical Research: Oceans*, *115*(C11). https://doi.org/10.1029/2010JC006306

Georgas, N., Blumberg, A., Herrington, T., Wakeman, T., Saleh, F., Runnels, D., Jordi, A., Ying, K., Yin, L., & Ramaswamy, V. (2016). The stevens flood advisory system: operational H3E flood forecasts for the greater New York/New Jersey metropolitan region. *Flood Risk Manag. Response*, *194*, 648-662.

Georgas, N., Yin, L., Jiang, Y., Wang, Y., Howell, P., Saba, V., Schulte, J., Orton, P., & Wen, B. (2016). An Open-Access, Multi-Decadal, Three-Dimensional, Hydrodynamic Hindcast Dataset for the Long Island Sound and New York/New Jersey Harbor Estuaries. *Journal of Marine Science and Engineering*, *4*(3), 48. https://www.mdpi.com/2077-1312/4/3/48

George, J., Ketcheson, D. I., & LeVeque, R. J. (2020). Shoaling on Steep Continental Slopes: Relating Transmission and Reflection Coefficients to Green's Law. *Pure and Applied Geophysics*, *177*(3), 1659-1674. https://doi.org/10.1007/s00024-019-02316-y

Greenspan, H. P. (1956). The generation of edge waves by moving pressure distributions. *Journal of Fluid Mechanics*, *1*(6), 574-592. https://doi.org/10.1017/S002211205600038X

Gurumurthy, P., Orton, P. M., Talke, S. A., Georgas, N., & Booth, J. F. (2019). Mechanics and Historical Evolution of Sea Level Blowouts in New York Harbor. *Journal of Marine Science and Engineering*, *7*(5), 160. https://www.mdpi.com/2077-1312/7/5/160

Haigh, I. D., Marcos, M., Talke, S. A., Woodworth, P. L., Hunter, J. R., Hague, B. S., Arns, A., Bradshaw, E., & Thompson, P. (2023). GESLA Version 3: A major update to the global higher-frequency sea-level dataset. *Geoscience Data Journal*, *10*(3), 293-314. https://doi.org/10.1002/gdj3.174

Harris, D. L. (1957). The Hurricane Surge. *Coastal Engineering Proceedings*, *1*(6), 5. https://doi.org/10.9753/icce.v6.5

Hope, M. E., Westerink, J. J., Kennedy, A. B., Kerr, P. C., Dietrich, J. C., Dawson, C., Bender, C. J., Smith, J. M., Jensen, R. E., Zijlema, M., Holthuijsen, L. H., Luettich Jr., R. A., Powell, M. D., Cardone, V. J., Cox, A. T., Pourtaheri, H., Roberts, H. J., Atkinson, J. H., Tanaka, S., . . . Westerink, L. G.

(2013). Hindcast and validation of Hurricane Ike (2008) waves, forerunner, and storm surge. *Journal of Geophysical Research: Oceans*, *118*(9), 4424-4460. https://doi.org/10.1002/jgrc.20314

Howarth, L. (1979). One hundred years of Lamb's Hydrodynamics. *Journal of Fluid Mechanics*, *90*(1), 202-207. https://doi.org/10.1017/S0022112079212159

Huang, N. E., Shih, H. H., Shen, Z., Long, S. R., & Fan, K. L. (2000). The ages of large amplitude coastal seiches on the Caribbean Coast of Puerto Rico. *Journal of Physical Oceanography*, *30*(8), 2001-2012.

Jay, D. A., & Flinchem, E. P. (1997). Interaction of fluctuating river flow with a barotropic tide: A demonstration of wavelet tidal analysis methods. *Journal of Geophysical Research: Oceans*, *102*(C3), 5705-5720. https://doi.org/10.1029/96JC00496

Jordi, A., Georgas, N., Blumberg, A., Yin, L., Chen, Z., Wang, Y., Schulte, J., Ramaswamy, V., Runnels, D., & Saleh, F. (2019). A Next-Generation Coastal Ocean Operational System: Probabilistic Flood Forecasting at Street Scale. *Bulletin of the American Meteorological Society*, *100*(1), 41-54. https://doi.org/10.1175/BAMS-D-17-0309.1

Kim, J., Choi, B.-J., & Omira, R. (2022). On the Greenspan resurgence of meteotsunamis in the Yellow Sea—insights from the newly discovered 11–12 June 2009 event. *Natural Hazards*, *114*(2), 1323-1340. https://doi.org/10.1007/s11069-022-05427-3

Kim, J., & Omira, R. (2024). Combined surge-meteotsunami dynamics: A numerical model for hurricane Leslie on the coast of Portugal. *Ocean Modelling*, *189*, 102368. https://doi.org/10.1016/j.ocemod.2024.102368

Landsea, C. W., & Franklin, J. L. (2013). Atlantic Hurricane Database Uncertainty and Presentation of a New Database Format. *Monthly Weather Review*, *141*(10), 3576-3592. https://doi.org/10.1175/MWR-D-12-00254.1

Latapy, A., Ferret, Y., Testut, L., Talke, S., Aarup, T., Pons, F., Jan, G., Bradshaw, E., & Pouvreau, N. (2023). Data rescue process in the context of sea level reconstructions: An overview of the methodology, lessons learned, up-to-date best practices and recommendations. *Geoscience Data Journal*, *10*(3), 396-425. https://doi.org/10.1002/gdj3.179

Leijala, U., Björkqvist, J. V., Johansson, M. M., Pellikka, H., Laakso, L., & Kahma, K. K. (2018). Combining probability distributions of sea level variations and wave run-up to evaluate coastal flooding risks. *Nat. Hazards Earth Syst. Sci.*, *18*(10), 2785-2799. https://doi.org/10.5194/nhess-18-2785-2018

Lilly, J. M., & Olhede, S. C. (2012). Generalized Morse Wavelets as a Superfamily of Analytic Wavelets. *Trans. Sig. Proc.*, *60*(11), 6036–6041. https://doi.org/10.1109/tsp.2012.2210890

Linares, Á., Bechle, A. J., & Wu, C. H. (2016). Characterization and assessment of the meteotsunami hazard in northern Lake Michigan. *Journal of Geophysical Research: Oceans*, *121*(9), 7141-7158. https://doi.org/10.1002/2016JC011979

Lobo, M., Jay, D. A., Innocenti, S., Talke, S. A., Dykstra, S. L., & Matte, P. (2024). Implementing Superresolution of Nonstationary Tides with Wavelets: An Introduction to CWT_Multi. *Journal of Atmospheric and Oceanic Technology*, *41*(10), 969-989. https://doi.org/10.1175/JTECH-D-23-0144.1

Marsooli, R., & Wang, Y. (2020). Quantifying Tidal Phase Effects on Coastal Flooding Induced by Hurricane Sandy in Manhattan, New York Using a Micro-Scale Hydrodynamic Model [Original Research]. *Frontiers in Built Environment*, *Volume 6 - 2020*. https://doi.org/10.3389/fbuil.2020.00149

Munk, W., Snodgrass, F., & Carrier, G. (1956). Edge Waves on the Continental Shelf. *Science*, *123*(3187), 127-132. https://doi.org/10.1126/science.123.3187.127

Mysak, L. A. (1980). Recent advances in shelf wave dynamics. *Reviews of geophysics*, *18*(1), 211-241. https://doi.org/10.1029/RG018i001p00211

Orton, P., Georgas, N., Blumberg, A., & Pullen, J. (2012). Detailed modeling of recent severe storm tides in estuaries of the New York City region. *Journal of Geophysical Research: Oceans*, *117*(C9). https://doi.org/10.1029/2012JC008220

Orton, P. M., Hall, T. M., Talke, S. A., Blumberg, A. F., Georgas, N., & Vinogradov, S. (2016). A validated tropical-extratropical flood hazard assessment for New York Harbor. *Journal of Geophysical Research: Oceans*, *121*(12), 8904-8929. https://doi.org/10.1002/2016JC011679

Ozsoy, O., Haigh, I. D., Wadey, M. P., Nicholls, R. J., & Wells, N. C. (2016). High-frequency sea level variations and implications for coastal flooding: A case study of the Solent, UK. *Continental Shelf Research*, *122*, 1-13.

Pasquet, S., & Vilibić, I. (2013). Shelf edge reflection of atmospherically generated long ocean waves along the central U.S. East Coast. *Continental Shelf Research*, *66*, 1-8. https://doi.org/10.1016/j.csr.2013.06.007

Pasquet, S., Vilibić, I., & Šepić, J. (2013). A survey of strong high-frequency sea level oscillations along the US East Coast between 2006 and 2011. *Natural hazards and earth system sciences*, *13*(2), 473-482.

Pattiaratchi, C. B., Bui, T., & Jankovic, I. (2022). The contribution of forerunner, meteotsunami, seiches and coastally trapped waves to storm surges. In *Australasian Coasts & Ports 2021: Te Oranga Takutai, Adapt and Thrive: Te Oranga Takutai, Adapt and Thrive* (pp. 752-758). New Zealand Coastal Society Christchurch, NZ.

Pawlowicz, R., Beardsley, B., & Lentz, S. (2002). Classical tidal harmonic analysis including error estimates in MATLAB using T_TIDE. *Computers & Geosciences*, *28*(8), 929-937. https://doi.org/10.1016/S0098-3004(02)00013-4

Pérez, B., Molina, I., & Peña, D. (2014). Outlier detection and robust estimation in linear regression models with fixed group effects. *Journal of Statistical Computation and Simulation*, *84*(12), 2652-2669. https://doi.org/10.1080/00949655.2013.811669

Pugh, D., & Woodworth, P. (2014). *Sea-Level Science: Understanding Tides, Surges, Tsunamis and Mean Sea-Level Changes*. Cambridge University Press. https://doi.org/10.1017/CBO9781139235778

Qiu, B., Miao, W., & Müller, P. (1997). Propagation and Decay of Forced and Free Baroclinic Rossby Waves in Off-Equatorial Oceans. *Journal of Physical Oceanography*, *27*(11), 2405-2417. https://doi.org/10.1175/1520-0485(1997)027<2405:PADOFA>2.0.CO;2

Rabinovich, A. B., Candella, R. N., & Thomson, R. E. (2013). The open ocean energy decay of three recent trans-Pacific tsunamis. *Geophysical Research Letters*, *40*(12), 3157-3162. https://doi.org/https://doi.org/10.1002/grl.50625

Ray, R. D., & Talke, S. A. (2019). Nineteenth-Century Tides in the Gulf of Maine and Implications for Secular Trends. *Journal of Geophysical Research: Oceans*, *124*(10), 7046-7067. https://doi.org/10.1029/2019JC015277

Redfield, A. C., & Miller, A. R. (1957). Water Levels Accompanying Atlantic Coast Hurricanes. In *Interaction of Sea and Atmosphere: A Group of Contributions* (pp. 1-23). American Meteorological Society. https://doi.org/10.1007/978-1-940033-15-0_1

Reid, R. O., & Bodine, B. R. (1968). Numerical Model for Storm Surges in Galveston Bay. *Journal of the Waterways and Harbors Division*, *94*(1), 33-57. https://doi.org/10.1061/JWHEAU.0000553

Staneva, J., Wahle, K., Koch, W., Behrens, A., Fenoglio-Marc, L., & Stanev, E. V. (2016). Coastal flooding: impact of waves on storm surge during extremes – a case study for the German Bight. *Nat. Hazards Earth Syst. Sci.*, *16*(11), 2373-2389. https://doi.org/10.5194/nhess-16-2373-2016

Stewart, R. H. (2008). *Introduction to physical oceanography* (Vol. 65). Texas A & M University College Station.

Talke, S. A., & Jay, D. A. (2013). Nineteenth Century North American and Pacific Tidal Data: Lost or Just Forgotten? *Journal of Coastal Research*, *29*(6a), 118-127. https://doi.org/10.2112/jcoastres-d-12-00181.1

Talke, S. A., & Jay, D. A. (2017). Archival water-level measurements: Recovering historical data to help design for the future.

Talke, S. A., Kemp, A. C., & Woodruff, J. (2018). Relative Sea Level, Tides, and Extreme Water Levels in Boston Harbor From 1825 to 2018. *Journal of Geophysical Research: Oceans*, *123*(6), 3895-3914. https://doi.org/10.1029/2017JC013645

Talke, S. A., Mahedy, A., Jay, D. A., Lau, P., Hilley, C., & Hudson, A. (2020). Sea Level, Tidal, and River Flow Trends in the Lower Columbia River Estuary, 1853–present. *Journal of Geophysical Research: Oceans*, *125*(3), e2019JC015656. https://doi.org/10.1029/2019JC015656

Talke, S. A., Orton, P., & Jay, D. A. (2014). Increasing storm tides in New York Harbor, 1844–2013. *Geophysical Research Letters*, *41*(9), 3149-3155. https://doi.org/10.1002/2014GL059574

Torrence, C., & Compo, G. P. (1998). A Practical Guide to Wavelet Analysis. *Bulletin of the American Meteorological Society*, *79*(1), 61-78. https://doi.org/10.1175/1520-0477(1998)079<0061:APGTWA>2.0.CO;2

Trinh, T. T., Pattiaratchi, C., & Bui, T. (2020). The Contribution of Forerunner to Storm Surges along the Vietnam Coast. *Journal of Marine Science and Engineering*, *8*(7), 508. https://www.mdpi.com/2077-1312/8/7/508

Ursell, F. (1952). Edge waves on a sloping beach. *Proceedings of the Royal Society of London. Series A. Mathematical and Physical Sciences*, *214*(1116), 79-97. https://doi.org/10.1098/rspa.1952.0152

Vennell, R. (2010). Resonance and trapping of topographic transient ocean waves generated by a moving atmospheric disturbance. *Journal of Fluid Mechanics*, *650*, 427-442. https://doi.org/10.1017/S0022112009993739

Wijeratne, E. M. S., & Pattiaratchi, C. B. (2024). Meteotsunamis Generated by Thunderstorms. *Journal of Geophysical Research: Oceans*, *129*(8), e2023JC020662. https://doi.org/10.1029/2023JC020662

Yankovsky, A. E. (2009). Large-scale edge waves generated by hurricane landfall. *Journal of Geophysical Research: Oceans*, *114*(C3). https://doi.org/10.1029/2008JC005113